Mixing and Demixing into MEMS

June 29, 2004

Contents

Chapter 1

Introduction

1.1 Overview

In this report will be described the experimental results obtained working on the problem of mixing and separation into MEMS (Micro Electro Mechanical System) and, when possible, the system modeling. Three principal phenomena are studied, phase segregation, regarding the separation of two miscible liquid, pulse mixing implemented trough micro osmotic flow, and electro kinetic instability for the mixing. All this method, apart the fascinating and complex physic they permit to explore, can be used fruitfully in different application, mostly, but not limited, to bio-medical engineering. The studies of device that can mix liquids into micro channels is requested were a very limited amount of substance is available, and a good mixing is needed for a

chemical reaction.

The main point prefixed is to differentiate from other actual developing technologies that use or moving parts inside their devices, or complex channel geometry. Instead the basic idea is to use the simplest geometry possible (T-Junctions and channels), while trying to modify the state of mixture with mainly electric force (or quenching, in the case of phase segregation, but this case can be brought back to first case).

Obeying this rule it is possible to achieve the goal to create cheap devices, that can be disposable, and small. As example, embedding this devices with chemical reactors, should be possible using a small amount of blood for blood analysis, and then trow the device away.

An important remark must be done about the scale on which we are working, about a tenth of millimeter that is big enough for the macroscale physic still apply, thus enabling us to understand easily some relationship (i.e. the pressure loss in a channel, defusing processes $\cdots$)

1.2 Structure

This report is structured into 3 more chapters, each for every experiment. In every chapter is briefly discussed the physic and the general notion present

in literature necessary to understand the problem; where is possible a preliminary discussion of the possible model is presented. The central part is covered the descriptions of the experiment setup and of the results found. In the last part of every chapter the results are discussed.

Chapter 2

Phase segregation of partially miscible mixtures

2.1 Scientific background

When a binary mixture with critical composition is quenched (or heated) from its single-phase region to a temperature below (above) the composition-dependent spinodal curve, it phase separates through a process called spinodal decomposition, which is characterized by the spontaneous formation of single-phase domains which then proceed to grow and coalesce [1]. Unlike nucleation, where an activation energy is required to initiate the separation, spinodal decomposition involves the growth of any fluctuations whose wavelength exceeds a critical value

Most of the experimental studies observed that, right after the temperature of the system has crossed that of the miscibility curve, the solution starts to separate by diffusion and coalescence, leading to the formation of well-defined patches, whose average concentration approaches its equilibrium value. Eventually, these patches become large enough that buoyancy dominates surface tension effects (i.e. the size R of these domains exceeds the capillary length) and the mixture separates by gravity. In general, from a simple dimensional analysis, we expect that the typical size of these domains should grow with time according to a power-law, i.e. $R \propto t^n$, with an exponent $n = 1/3$ when diffusion is the dominant mechanism of material transport [2], while when hydrodynamic, long-range interactions become important we find either $n = 1$ or $n = 2/3$, depending, respectively, whether viscous or inertial forces are dominant [3, 4]. This theoretical analysis is in good agreement with most of the experimental studies of the spinodal decomposition of liquid mixtures, where it is shown that, after a short initial stage where $R \propto t^{1/3}$, the size of the single-phase domains grows linearly with time, i.e. $R \propto t$ [5, 6]. Since in these experiments the mixtures completed their phase separation process before reaching the final, inertia-dominated stage, the scaling $R \propto t^{2/3}$ was never observed.

Based on the diffuse interface model [7, 8, 9], Mauri and coworkers [10, 11, 12, 13] have simulated the phase separation of regular mixtures, finding that

a) phase segregation is driven by convection, and not by diffusion neither by gravity, so that the typical drop size grows linearly with time; b) during most of the phase segregation process the system is far from local equilibrium, explaining why we observe bulk motion even when the system is composed of nucleating drops with sharp interfaces (trivially, no bulk flow would exist if they were at equilibrium).

In the present study, we want to investigate whether phase segregation can result in large-scale convection, dominating all capillary-driven and gravity effects. To do that, instead of using narrow glass cells, we introduced in a long capillary tube a quasi isopycnic partially miscible liquid mixture, which separates into two phases having densities differing by less than 0.5% from each other, so that gravity effects could be ruled out. At the end, we showed that large scale convection drives phase segregation, leading to the formation of two phases axially separated from each other, i.e. with the formation of interfaces that are perpendicular to the capillary walls. In addition, such process takes place within less than a tenth of a second, thereby suggesting that it could be employed as a switching device.

2.2 Experimental setup

An experimental setup was designed and built to allow the observation of the phase separation process in the size range of $10\,\mu m$ to 1 mm. It consisted of a $1\,mm$-wide, $0.5\,mm$-deep, $30\,cm$-long microchannel, whose temperature was regulated by Peltier effect, as two opposite walls of the microchannel were made of aluminium and connected to a voltmeter.

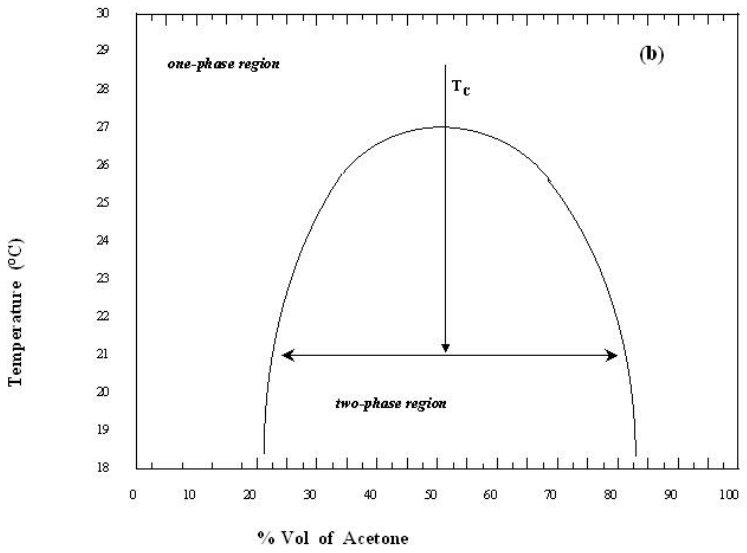

Figure 2.1: Phase Diagram of 50% acetone - 50% hexadecane liquid mixture

In our experiments we used a 50% acetone - 50% hexadecane (in volume)

critical liquid mixture [14], whose phase diagram is represented in Figure 2.1, with a critical temperature of $T_c = 27^oC$. At ambient temperature, this mixture separates into two phases, with a density difference $\Delta\rho = 6 \times 10^{-4} g/cm^3$ that, although very small, is still sufficient to cause a slow separation of a droplet dispersion by settling and coalescence. Similar, so called, isopycnic mixtures have been also used by Guenoun et al. [5]. In addition, $100\,ppm$ of crystal violet, a dye that absorbs preferentially in acetone, were added to the mixture to enhance the visualization of the process. When dissolved in such small percent, this dye does not change the phase diagram of the mixture, or the characteristics of the phase separation process.

In all our experiments, the mixture was initially heated to 45^oC and then cooled back to 15^oC with a $2^oC/s$ quenching rate. The kinetics of the phase separation process was observed using a digital camera with high resolution, mounted on a microscope (see Figure 2.2).

2.3 Experimental results

First of all, since the mixture must be confined within the microchannel, the two ends of the microchannel must be accurately clamped, to avoid spills. In addition, in order to reduce capillary effects, the microchannel walls should be made of glass, instead of plexiglass. At this point, performing the experiment,

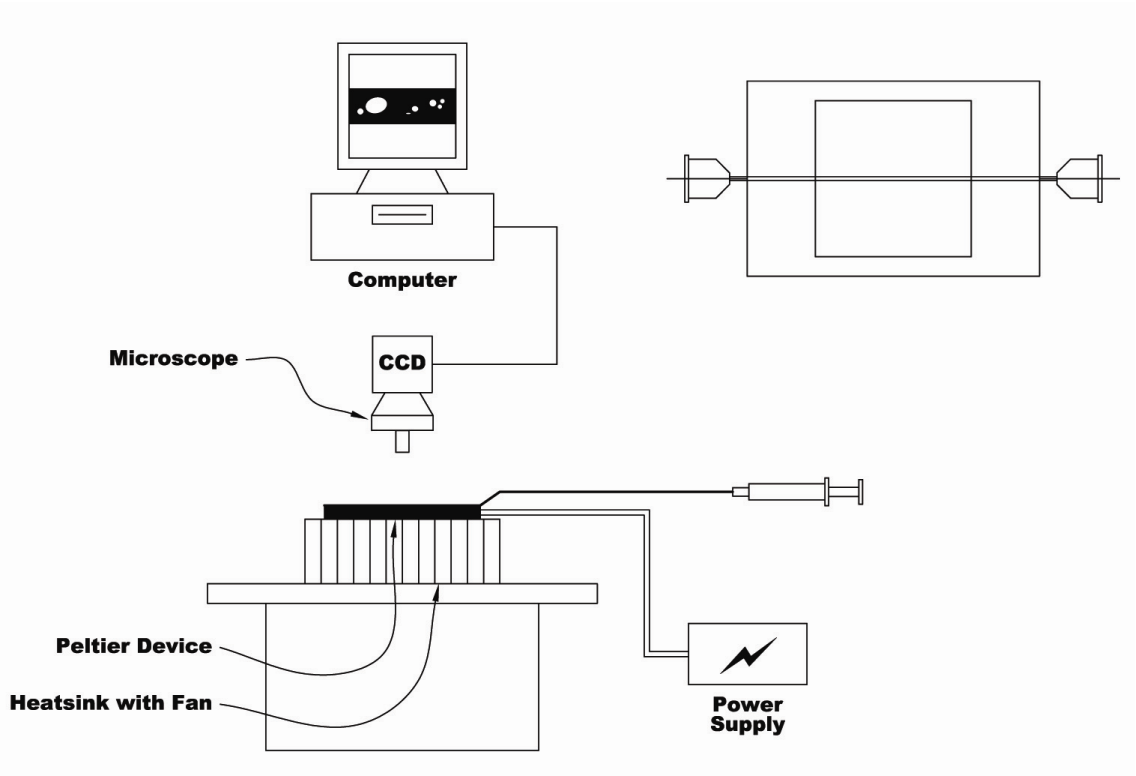

Figure 2.2: Experiment setup

we saw that right after the quench large, mm-size acetone-rich drops form and start to move axially at speeds exceeding $0.3\,mm/s$. Example of this phenomenon are reported in Figures 2.3, 2.4 and 2.5. Eventually, a very neat interface between the two phases is formed, as shown in Figure 2.6 (note that the different color between the photos is due to the camera auto brightness).

From this experiment is also possible to see the tendency of the drops of the same phase to coalesce as they touch each other, (naturally, provided that the temperature remains below the critical temperature), as shown in Figure 2.7. Similar effects were observed previously [14, 15, 16]. In particular, Gupta *et al.* [17] have shown that such strong coalescence occurs even when surfactants are added to the mixture.

2.4 Conclusions and discussion

In this work the phase segregation of isopycnic, partially miscible liquid mixtures in microchannels has been observed. We have seen that the process takes place through the formation of $100\,\mu m$ drops that move axially and coalesce. As the drop speed is quite large (i.e. larger than $0.3mm/s$), complete phase segregation can be achieved very quickly, suggesting that it might be possible to apply this phenomenon to build micro-switching devices.

A partial explanation of this effect is provided by the diffuse interface model [7, 8, 9, 12, 18], predicting that convection in systems far from equilibrium, such as ours, is driven by chemical potential gradients. Consequently, the acetone-rich drops will attract each other [17], thereby explaining the observed strong coalescence among drops. As for the movement of the drops, we believe that it follows the week temperature gradient existing along the axial direction. This, however, should not be mistaken by thermocapillary motion, since this force would induce drop speeds that are a few order of magnitude smaller than the ones that we observe. In any case, further studies are required to explain the strong drop migration that is observed experimentally.

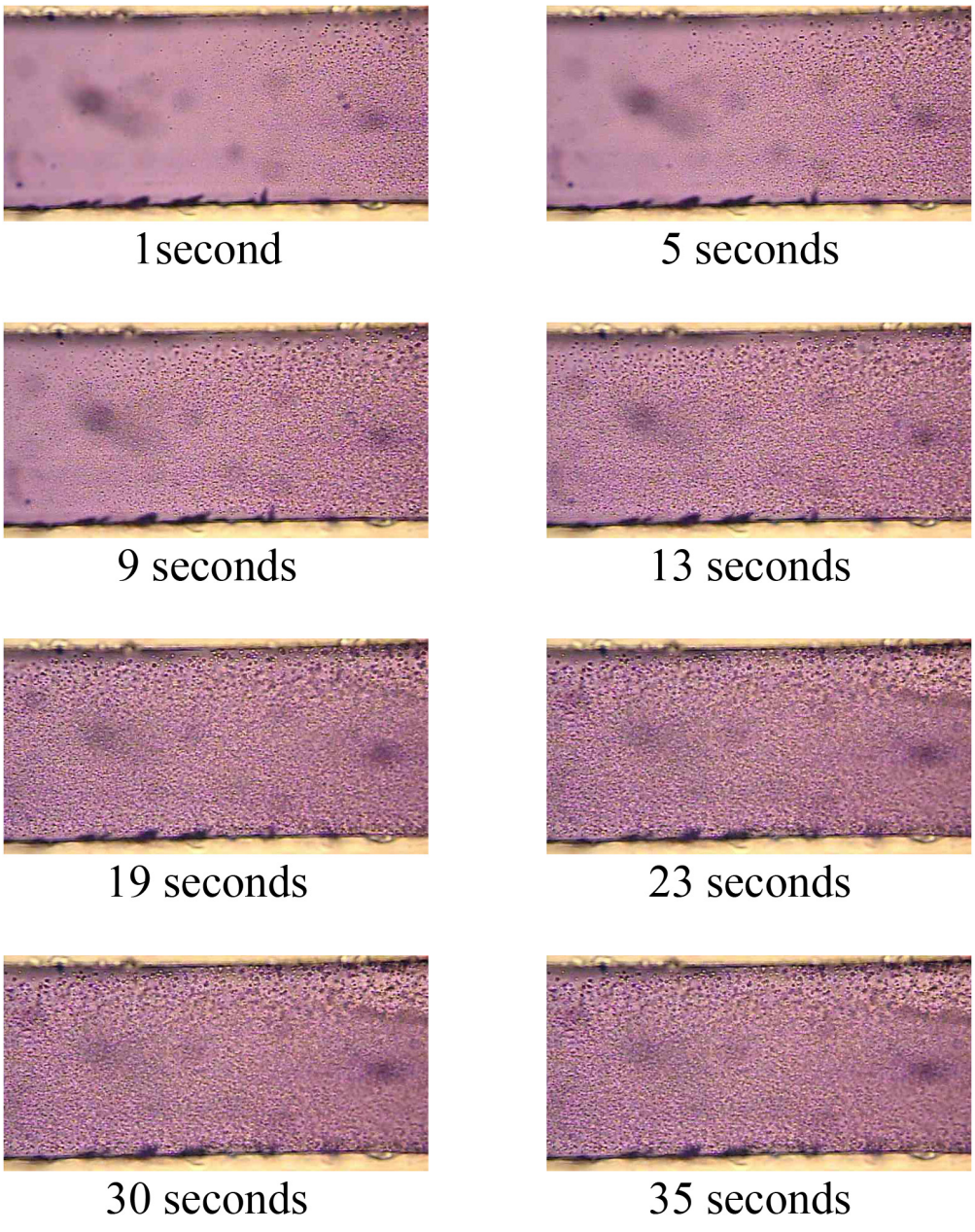

Figure 2.3: Phase Separation pictures

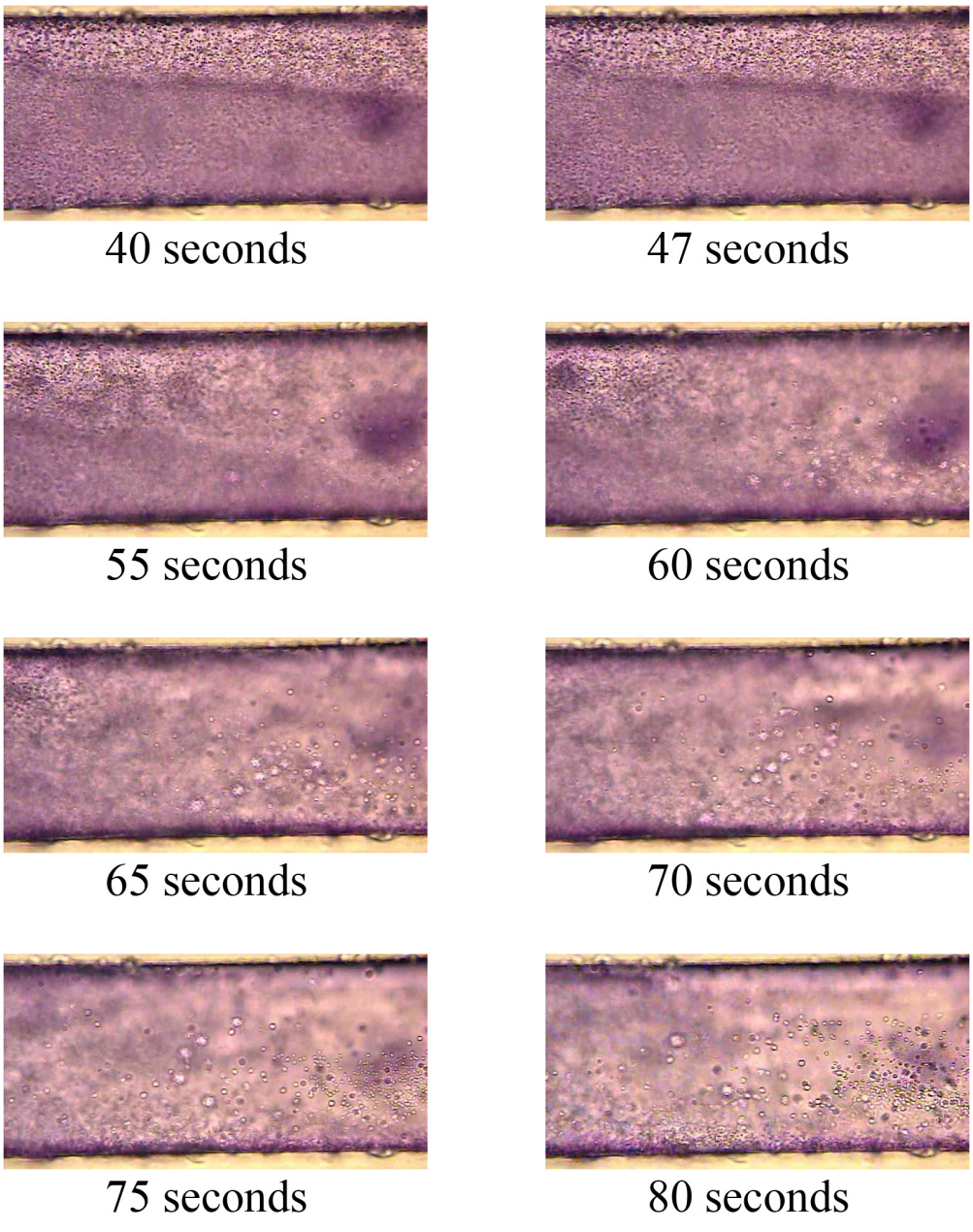

Figure 2.4: Phase Separation pictures

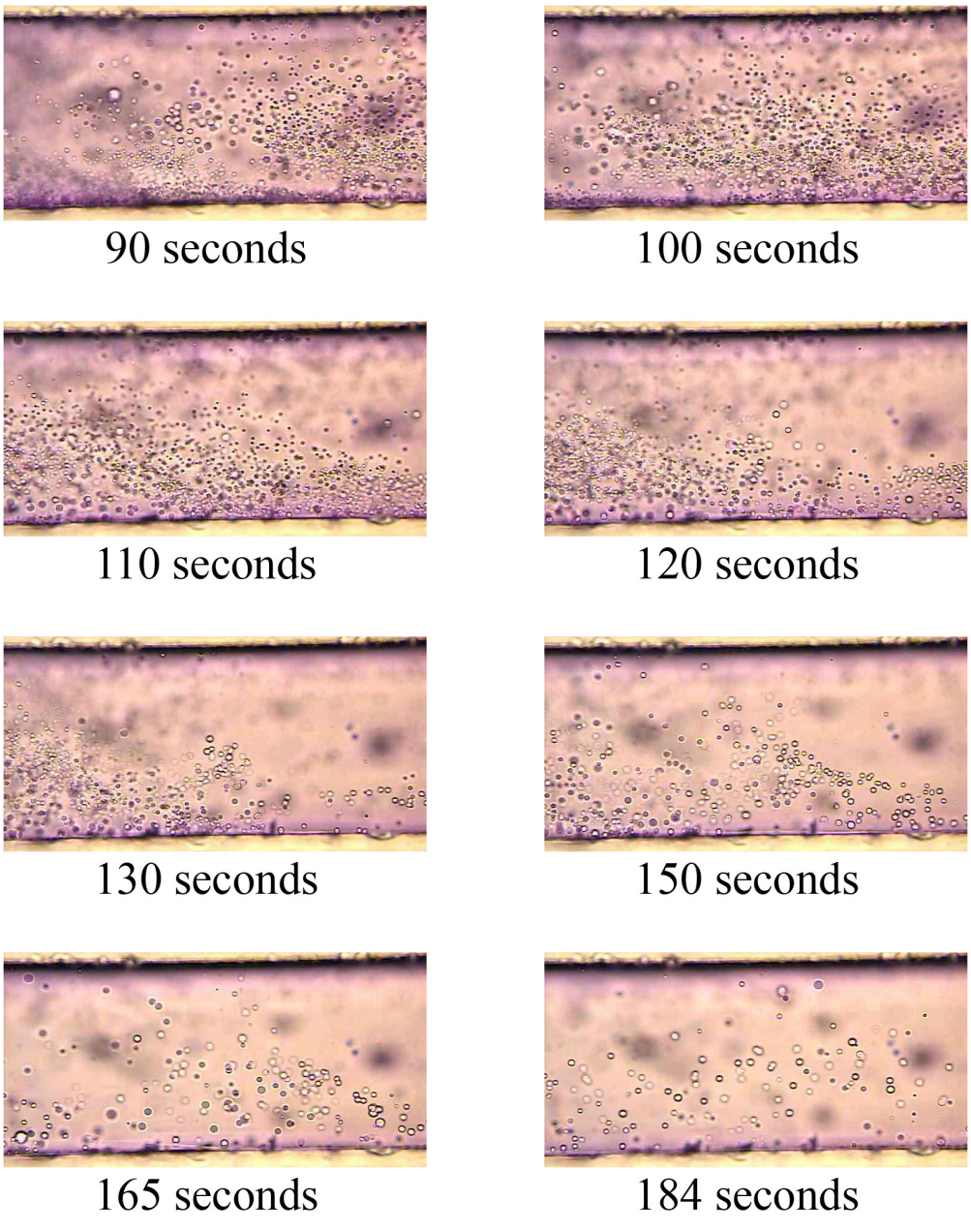

Figure 2.5: Phase Separation pictures

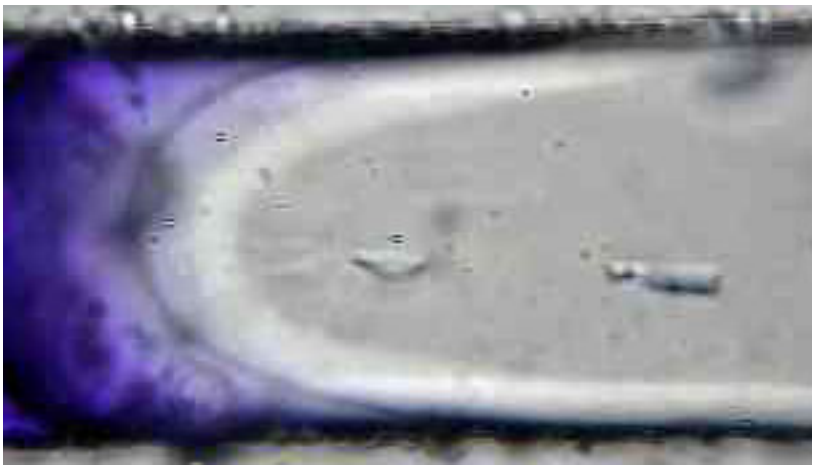

Figure 2.6: Interface after the mixture reaches the equilibrium

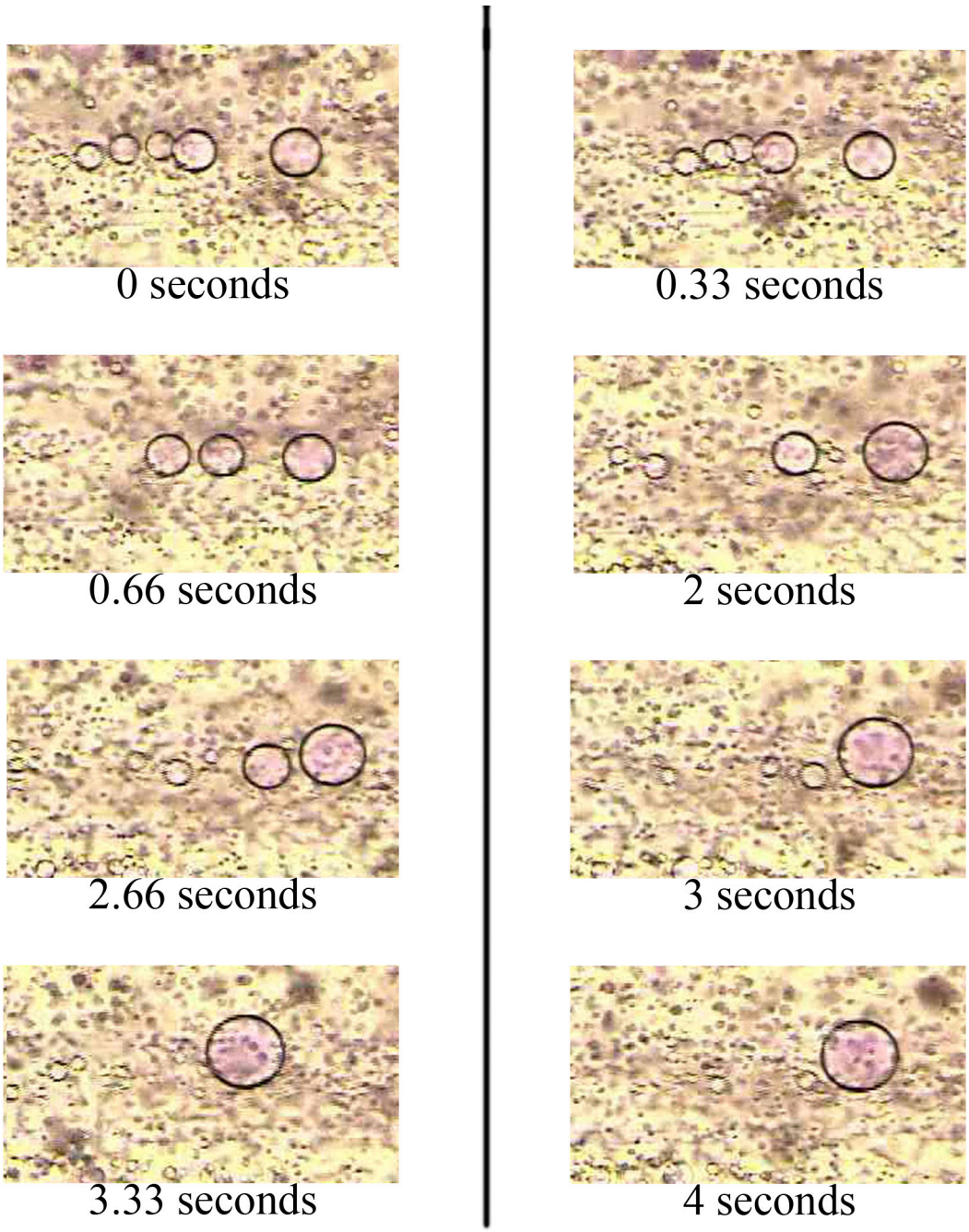

Figure 2.7: Phase Separation pictures

Bibliography

[1] Reviews on spinodal decomposition can be found in: J.S. Langer, in *Systems Far from Equilibrium*, L. Garrido, ed., Lecture Notes on Physics No. 132, Springer Verlag, Berlin (1980); J.D. Gunton, M. San Miguel & P.S. Sahni, in *Phase Transition and Critical Phenomena*, Vol. 8, C. Domb & J.L. Lebowitz, eds., Academic Press, London (1983).

[2] E.M. Lifshitz and L.P. Pitaevskii, *Physical Kinetics*; Pergamon Press: New York, 1984; Chapter 12.

[3] E. Siggia, "Late stages of spinodal decomposition in binary mixtures," Phys. Rev. A **20**, 595 (1979).

[4] H. Furukawa, "Role of inertia in the late stage of the phase separation of a fluid," Physica A **204**, 237 (1994).

[5] P. Guenoun, R. Gastaud, F. Perrot and D. Beysens, "Spinodal decomposition patterns in an isodensity critical binary fluid: direct-visualization

and light-scattering analyses," Phys. Rev. A **36**, 4876 (1987).

[6] F. Califano and R. Mauri, "Drop size evolution during the phase separation of liquid mixtures," Ind. Eng. Chem. Res. **43**, 349 (2004).

[7] P.C. Hohenberg and B.I. Halperin, "Theory of dynamic critical phenomena," Rev. Mod. Phys. **49**, 435 (1977).

[8] D.M. Anderson, G.B. McFadden and A.A. Wheeler, "Diffuse-interface methods in fluid mechanics," Annu. Rev. Fluid Mech. **30**, 139 (1998).

[9] J. Lowengrub and L. Truskinovsky, "Quasi-incompressible Cahn-Hilliard fluids and topological transitions," Proc. R. Soc. London, Ser. A **454**, 2617 (1998).

[10] N. Vladimirova, A. Malagoli and R. Mauri, "Diffusio-phoresis of two dimensional liquid droplets in a phase separating system," Phys. Rev. E **60**, 2037 (1999).

[11] N. Vladimirova, A. Malagoli and R. Mauri, "Two-dimensional model of phase segregation in liquid binary mixtures," Phys. Rev. E **60**, 6968 (1999).

[12] N. Vladimirova, A. Malagoli and R. Mauri, "Two-dimensional model of phase segregation in liquid binary mixtures with an initial concentration gradient," Chem. Engng. Sci. **55**, 6109 (2000).

[13] A.G. Lamorgese and R. Mauri, "Phase separation of liquid mixtures," in *Non-Linear Dynamics and Control in Process Engineering - Recent Advances,* G. Continillo, S. Crescitelli and M. Giona eds., Springer, Berlin (2002), pp. 139-152.

[14] G. Santonicola, R. Mauri and R. Shinnar, "Phase separation of initially non-homogeneous liquid mixtures," Ind. Eng. Chem. Res. **40**, 2004 (2001).

[15] H. Tanaka, "Coarsening mechanisms of droplet spinodal decomposition in binary fluid mixtures," J. Chem. Phys. **105**, 10099 (1996).

[16] R. Mauri, F. Califano, E. Calvi, R. Gupta and R. Shinnar, "Convection-driven phase segregation of deeply quenched liquid mixtures," J. Chem. Phys. **118**, 8841 (2003).

[17] R. Gupta, R. Mauri and R. Shinnar, "Phase separation of liquid mixtures in the presence of surfactants," Ind. Eng. Chem. Res. **38**, 2418 (1999).

[18] D. Jacqmin, "Contact-line dynamics of a diffuse fluid interface," J. Fluid Mech. **402**, 57 (2000).

Chapter 3

Electrokinetic micro flow instability

3.1 Introduction

When two miscible liquids are brought in contact with each other, they mix by convection and by diffusion. In the absence of any convective process, mixing is very slow. For example, two fluids in a $100\mu m$ width microchannel diffuse into one another with times of $O(1\,min)$. Naturally, in the presence of external forces that are strong enough to override surface tension, mixing is much faster. Unfortunately, most of these convection-inducing external forces, such as gravity, are body forces and therefore in microdevices their effect is overridden by surface forces, which tend to stop mixing altogether.

The objective of this work is to show that fluid mixing can be enhanced by applying a DC uniform field, provided that the two fluids to be mixed have different electrical conductivity. In this case, on the sharp interface initially separating the two fluids, a surface force will be induced, which is proportional to the gradient of the electric-field intensity. This force triggers an instability that breaks the interface and strongly enhances the mixing process.

The fluids to be mixed are pure corn oil and dyed corn oil (with Acros Organics oil red O), where the latter is doped with a conductive doper in a ratio of 25% volume. The used dopant is oil miscible, antistatic, Stadis 450, that increases the electrical conductivity and permittivity. The corn oil density and viscosity are $\rho = 0.992 \times 10^3 kg/m^3$, and $\eta = 6 \times 10^{-2} kg/m$. Permittivity and conductivity measurements has been done in [1], through in a AC regime, showing that the doped oil permittivity and conductivity is 4 order bigger than the pure oil one for low frequency (it's reasonable to assume that for in DC regime the permittivity and conductivity of pure oil is negligible). In Figure 3.1 we report the obtained data. The two fluids have the same mechanical qualities, but different electrical proprieties, such as conductivity and permittivity. The experiments have been performed using two different devices, the first having only a small electrode surface, the second with a long pair of electrodes placed into the outlet channel walls.

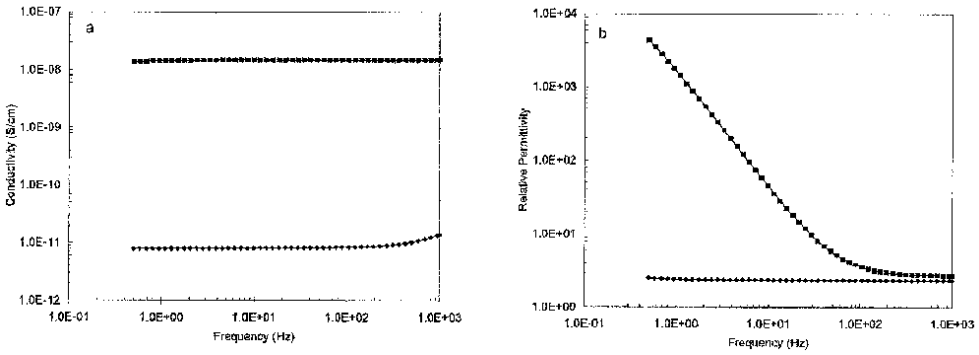

Figure 3.1: Permittivity and conductivity of pure corn oil (diamonds) and doped oil (squares). Data published in [1]

Both devices present a T-junction, with two inlets and one outlet. The two oil flows enter the inlets by gravity, since they are stored into a pair of syringes which are held above the device; then they flow into the main channel and out, each occupying half of the channel, flowing at low Reynolds number.

3.2 First experiment

3.2.1 Experimental setup

In this experiment, we used a 5cm x 3cm device, with small electrodes mounted on the borders of the outlet channel; the electrodes consist of 1/4 millimeter diameter brass wires, with one end assembled into the channel walls, as shown in Figure 3.2.In this experiment only the first couple are used, while the other 4 are used as a visual reference for distance. The wires

have a $250\mu m$ diameter and are spaced 5mm from each other.

3.2.2 Results

When the applied voltage remains below a certain threshold value, nothing seems to happen at the electrodes where the voltage is applied. On the other hand, when the applied voltage is larger than this threshold, the interface between the two liquids presents a time periodic perturbation. In addition, changing the polarity of the electric field seems to have no effects. This result shows that it is possible to provide enough energy to break the surface tension at the interface, without causing turbulence.

In Figure 3.3 we present 10 images at five different electrodes, from the most upstream (left-side column) to the most downstream (right-side column), showing the behavior of the system when no voltage is applied (upper row) and when a 101.5 voltage is applied (lower row) to the first couple of electrodes. At a glance, the effect of mixing is quite visible. The change of color of the clear part is due to the auto-brightness function of the camera. These images have been elaborated, first extracting the red channel intensity and reducing each picture to an 8 bit-depth gray scale image, then cutting the channel walls out and defining the following normalized concentration index at the 5 sections:

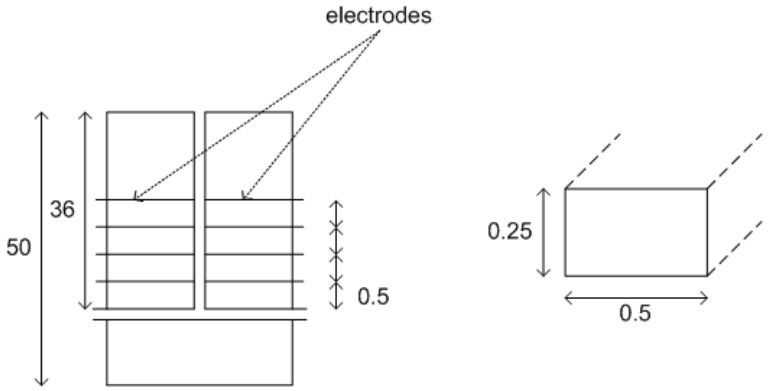

Figure 3.2: First experiment device drawing

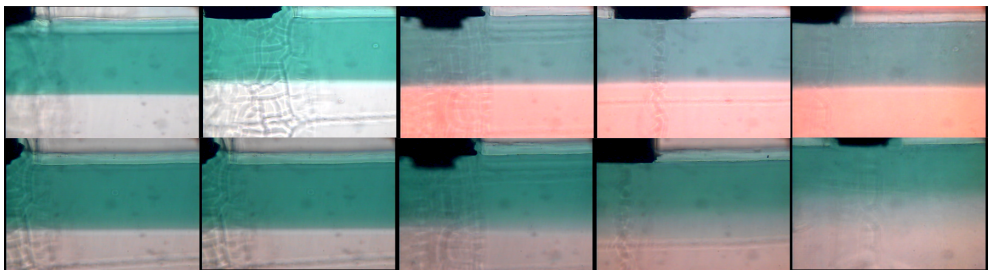

Figure 3.3: Images at the five electrodes, from the most upstream (left-side column) to the most downstream (right-side column), when no voltage is applied (upper row) and when a 101.5 voltage is applied (lower row) to the first couple of electrodes.

$$c(y,s) = \frac{R(y,s) - R_{min}(s)}{R_{max}(s) - R_{min}(s)}$$

Here $R(y,s)$ is the red channel intensity at section s ($s = 1, ..., 5$) and at a distance y from the wall, while $R_{min}(s)$ and $R_{max}(s)$ represent the maximum and minimum value of the red channel intensity at section s. Plotting the concentration index $c(y,s)$, whose value lays between 0 and 1, Figure 3.4 is obtained. A rudimental and qualitative value of the degree of mixing can be obtained by comparing the distance between the 40% and 80% of the c value, as shown in Figure 3.5.

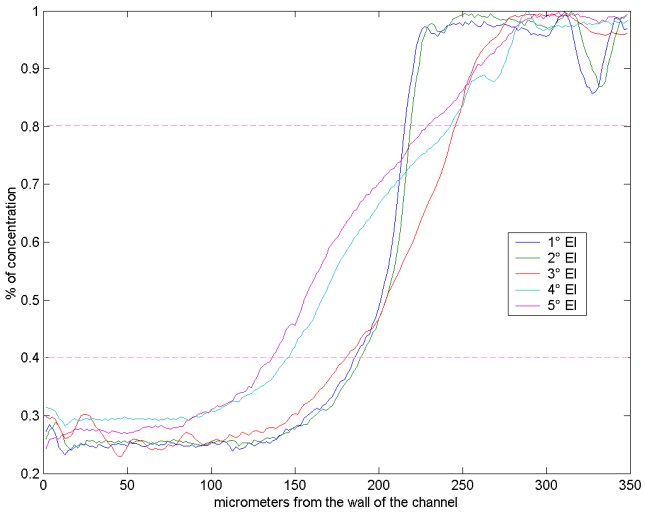

Figure 3.4: Concentration index at the 5 electrodes couple, versus the distance of the channel wall, along a section of the channel.

Note that, since the flow speed is about $0.6\,mm/s$ and the distance between the first and the last electrode is $20\,mm$, the characteristic timescale of the process is $30\,s$. The typical flow velocity was obtained both by measuring the speed of suspended tracer particles and by directly measuring the volumetric flux.

3.2.3 Conclusion

This first experiment shows that it is actually possible to break the interface between two liquids without causing any turbulence. Such interface breaking induces an accelerated mixing that is similar to diffusive mixing, but with shorter timescale. Since changing the polarity doesn't have any effects, we conjecture that this effect is related to the energy of the electric field, and, probably, to the exposure time. Consequently, we decided to use a longer electrode, so that the same effect could be achieved with lower tensions.

3.3 Second experiment

3.3.1 Experimental setup

The second device has longer electrodes, made of titanium, built into the outlet channel walls. The channel width is unvaried, compared to the previ-

ous experiment, although the section now is square. As in the previous case, the liquid flows are driven by gravity, and the their ratio is half and half; a schematic of this device is presented in Figure 3.6

3.3.2 Results

The tensions used are lower than $40V$, since higher energies cause the liquid to behave turbulently. The most evident difference from the previous case is that, while in the first experiment the electric field is used only to catalyze the instability and break the interface, here it is actually the field that moves the two liquids and makes them mix, so that it is possible to see the mixing inside the field of view. In Figure 3.7 the morphology of the phenomenon is shown, with the first number representing the distance downstream from the point where the electrodes start (it is possible to see this point on the left side of the first image), and the second the voltage applied.

3.3.3 Image analysis

In this case, the concentration at each point is determined by adding the intensities of all three channels (instead of considering only the red channel, as in the previous experiment), as shown in the MatLab code below. As before, the images were cleaned from the effect of the non-uniform microscope light

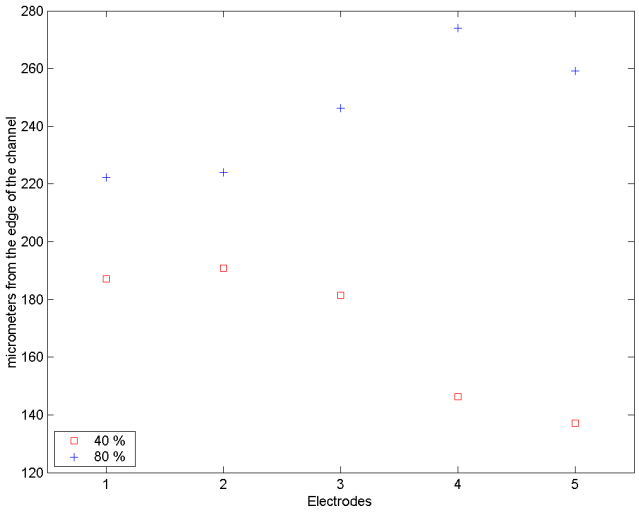

Figure 3.5: Representation of the 40% and 80% of c at each electrode couples.

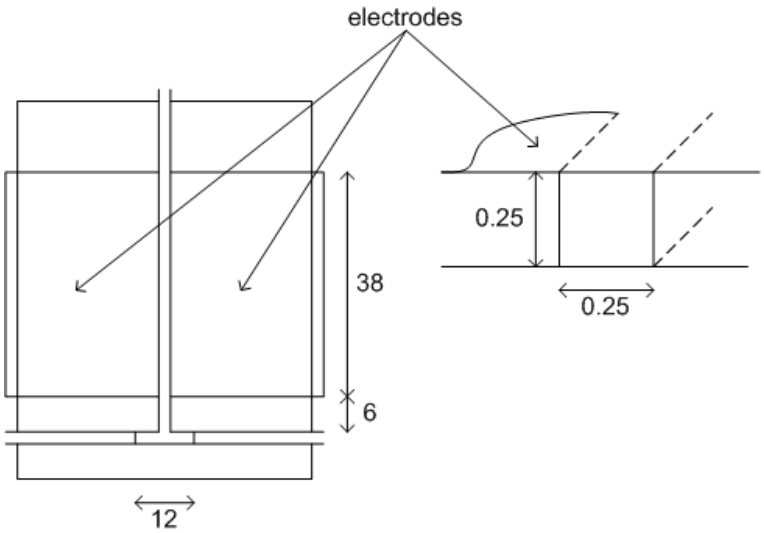

Figure 3.6: Representation of the 40% and 80% of c at each electrode couples

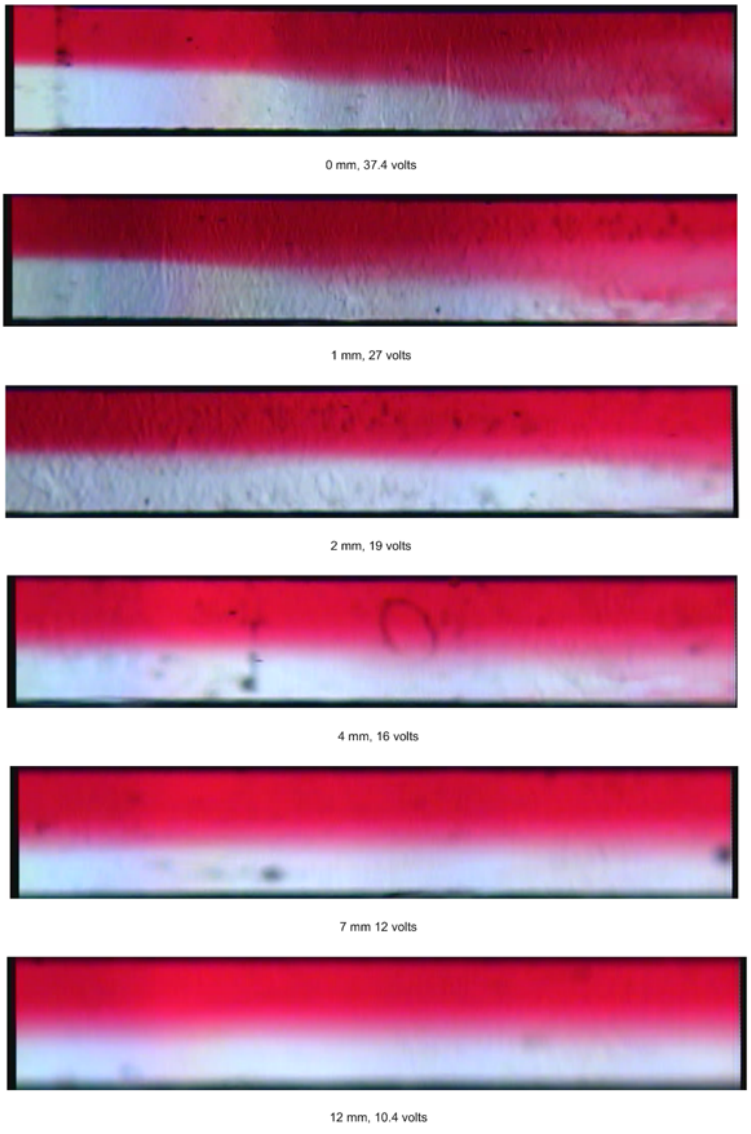

Figure 3.7: Pictures of the channel; the first value represent the distance downstream from the start of the electrodes, the second the voltage applied.

and of the background noise; in addition, only the center part of each image was used, discarding the channel walls. Each images has been normalized in two different ways: if the image shows both liquids along all the channel, every vector is normalized with his maximum and minimum value along the section, since it's expected that all the scale, from 0 to 1, is covered. Instead, where the mixing is stronger, the second half of the channel is normalized with the maximum and minimum value of the first half. Although this method could cause some data to be slightly outside of the $0 - 1$ range, error is negligible. The data obtained were plotted into a three dimensional graphs (Figures 3.8, 3.9, and 3.10). At this point, as in earlier works [1], we define the degree of mixing as the standard deviation of the color intensity fluctuations, $I(x)$, within a section of the channel, at a distance x from the inlet,

$$\delta_m(x) = 1 - \frac{I(x)}{I(0)},$$

where the liquid at the inlet is supposed to be unmixed (i.e. with $\delta_m(0) = 0$). The resulting plots are shown in Figure 3.11.

3.4 MatLab code

In the previous analysis we used the following code. Again, note that the concentration at each point is obtained using all three channels, by summing the three intensities and then subtracting the minimum value. If, as in this

case for the blue channel, a channel has an almost constant value in all the picture, then that value is filtered out anyway.

```
function Cchopped=  Liu3d (name)

    r=1;
    g=1;
    b=1;
    im=imread(name);
    R=double(im(:,:,1))*r;
    G=double(im(:,:,2))*g;
    B=double(im(:,:,3))*b;
    ColoreSum=R+G+B;
    for i=51:650
        for j=16:115
        Cchopped(i-50,j-15)=ColoreSum(i,j);
        end
    end

    for i=1:length(Cchopped)
```

```
    echo on
    M=max(Cchopped(i,:));
    m=min(Cchopped(i,:));
    echo off
    Cchopped(i,:)=(Cchopped(i,:)-m)/(M-m);

end
figure
h=surf(Cchopped);
set(gca,'XTick',[0  100])
set(gca,'YTick',[0 300 600])
set(gca,'XTickLabel',[0  0.250])
set(gca,'YTickLabel',[0 0.750 1.5])
xlabel('Channel tickness (mm)')
ylabel('Channel length (mm)')
shading interp;
set(gca,'PlotBoxAspectRatio',[1 6 1]);
view(55,20);
title(name);

BV=0.45;
```

```
    for i=1:600;
        v(i)=1-(sqrt(var(Cchopped(i,:))))/BV;
    end

    figure
    plot (v);
    set(gca,'XTick',[0 300 600]);
    set(gca,'XTickLabel',[0 0.750 1.5]);
    xlabel('Channel length (mm)');
    ylabel('Mixing index (%)');
    axis([-inf,inf,0,1]);
    title(name);
end

%function used for images that doesn't have
% all the colors in the last sections
%the max e min for the second half is
%calculated as the max and min of the firs half

function Cchopped=  Liu3d (name);
```

```
r=1;

g=1;

b=1;

im=imread(name);

R=double(im(:,:,1))*r;

G=double(im(:,:,2))*g;

B=double(im(:,:,3))*b;

ColoreSum=R+G+B;

 for i=51:650

    for j=16:115

    Cchopped(i-50,j-15)=ColoreSum(i,j);

    end

end

M=0;

m=1000;



end


for i=1:length(Cchopped)
```

```
    if i<length(Cchopped)/2
        M=max(max([M Cchopped(i,:)]));
        m=min(min([m Cchopped(i,:)]));
    end;

    Cchopped(i,:)=(Cchopped(i,:)-m)/(M-m);

end
figure
title(name)
h=surf(Cchopped);
set(gca,'XTick',[0  100])
set(gca,'YTick',[0 300 600])
set(gca,'XTickLabel',[0  0.250])
set(gca,'YTickLabel',[0 0.750 1.5])
xlabel('Channel tickness (mm)')
ylabel('Channel length (mm)')

shading interp;
set(gca,'PlotBoxAspectRatio',[1 6 1]);
view(55,20);
```

```
    BV=0.45;
    for i=1:600;
        v(i)=1-(sqrt(var(Cchopped(i,:))))/BV;
    end


    figure
    title(name);
    plot (v);
    set(gca,'XTick',[0 300 600]);
    set(gca,'XTickLabel',[0 0.750 1.5]);
    xlabel('Channel length (mm)');
    ylabel('Mixing index (%)');
    axis([-inf,inf,0,1]);


end
```

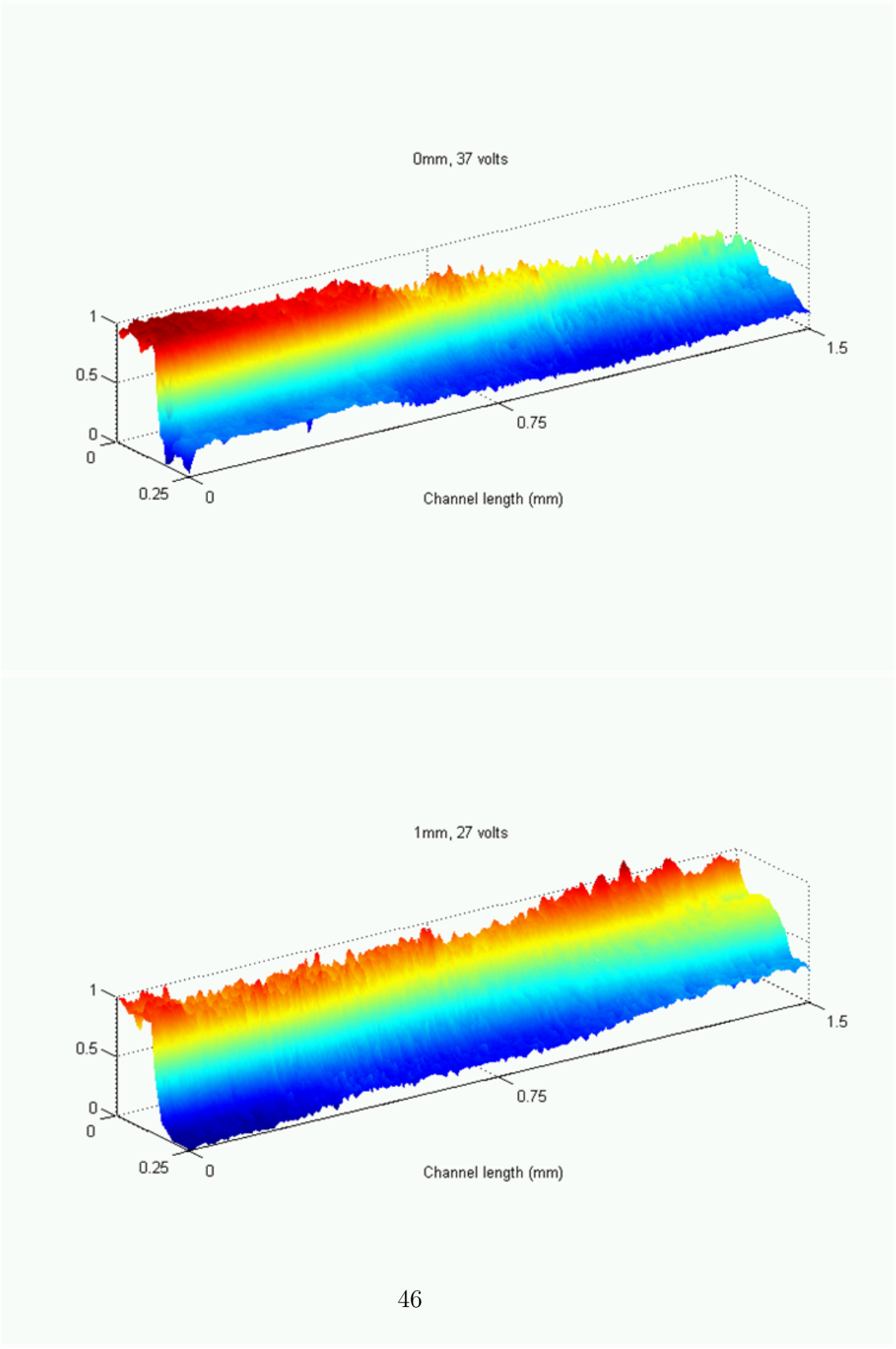

Figure 3.8: Three dimensional representation of the normalized red channel intensity from Figure 3.7 picture.

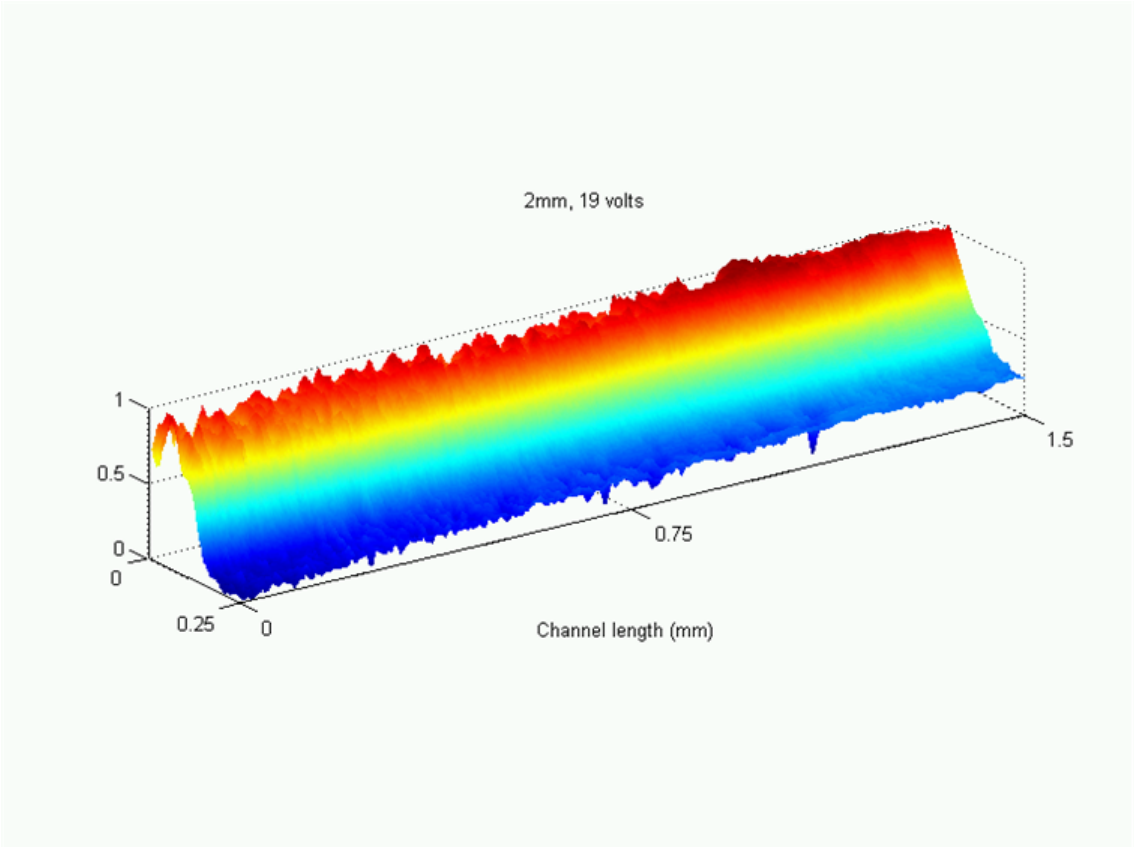

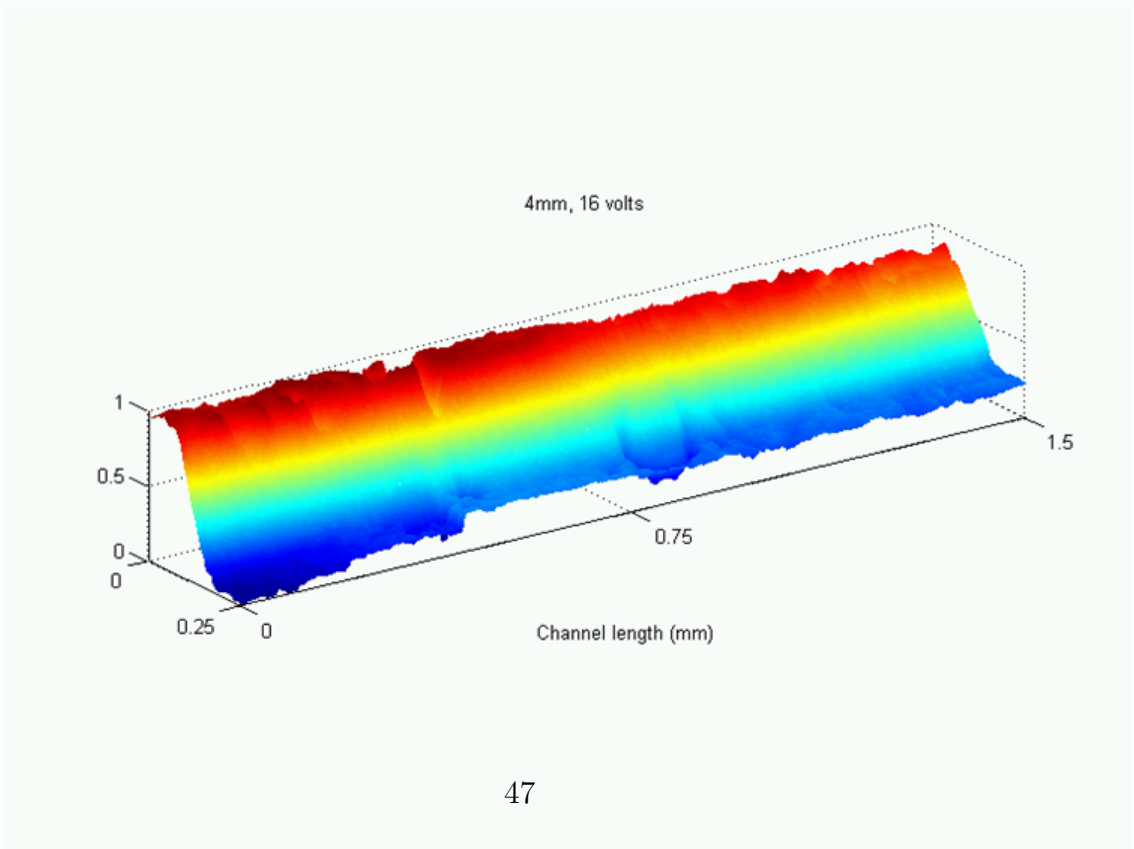

Figure 3.9: Three dimensional representation of the normalized red channel intensity from Figure 3.7 picture.

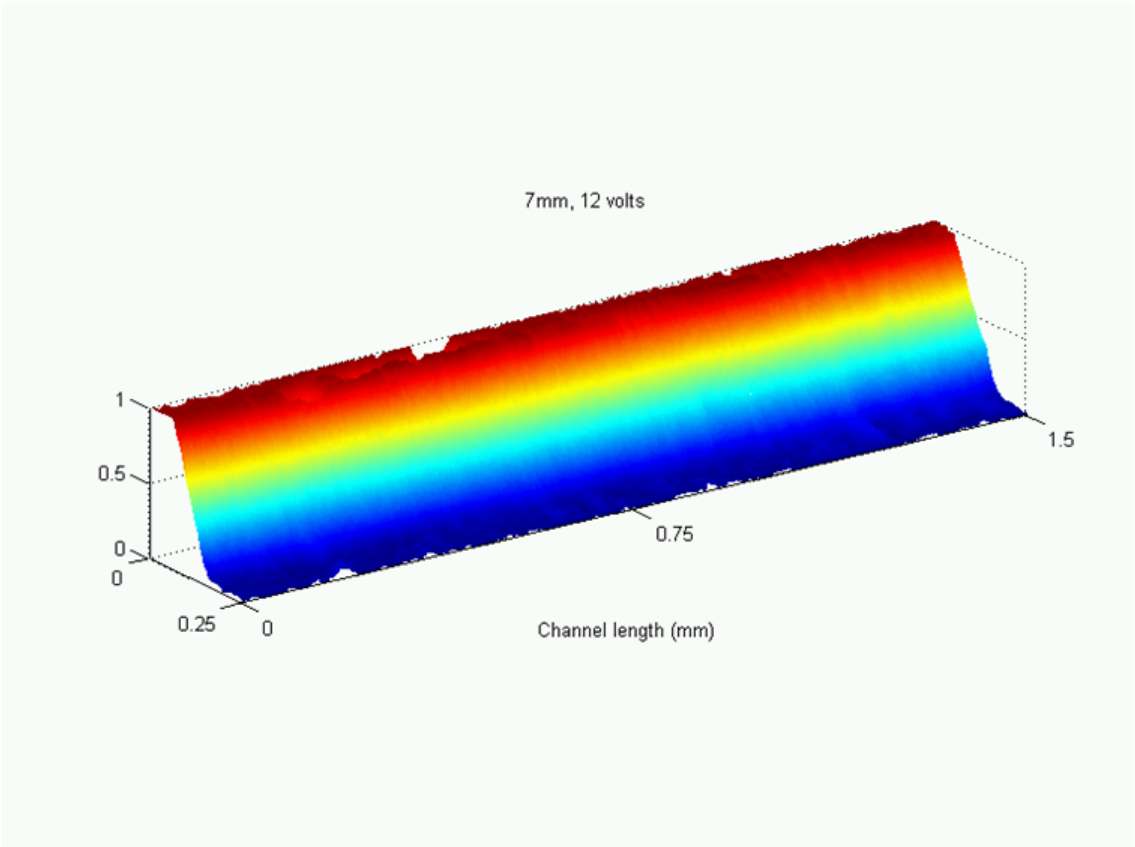

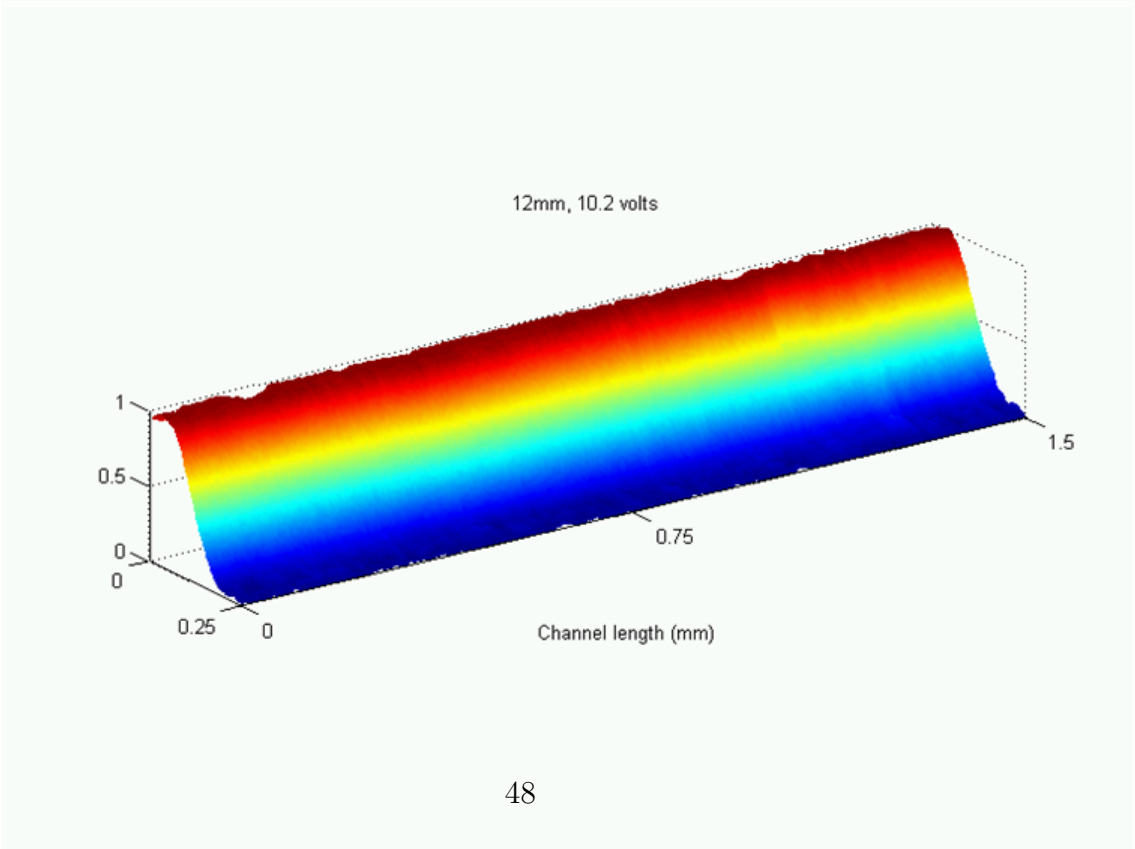

Figure 3.10: Three dimensional representation of the normalized red channel intensity from Figure 3.7 picture.

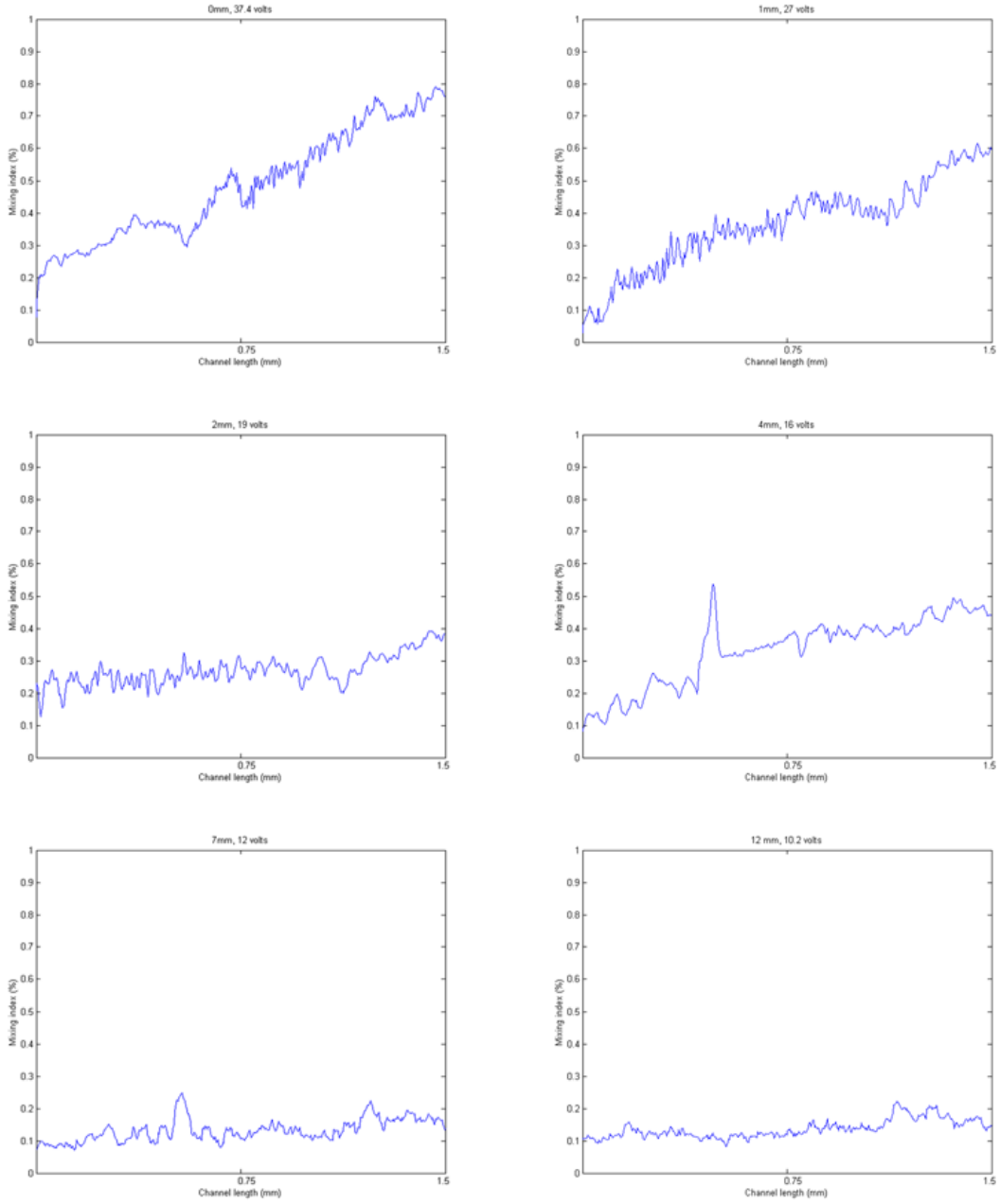

Figure 3.11: Plotting of the mixing index from each data set represented in Figures 3.8, 3.9, and 3.10

3.4.1 Results

The plots of the mixing index are extremely noisy, but they clearly show that δ_m depends linearly on the distance x from the inlet. In fact, approximating δ_m as a straight line from 0 at $x = 0$ to a maximum value at $x = \ell$, where ℓ is the length of the channel, we obtained the following table:

$Volts$	x (mm)	$\delta_m(x, Volts)$	$m = \delta_m(x, Volts)/x$
37.4	1.5	0.8	0.53
27	2.5	0.6	0.24
19	3.5	0.35	0.1
16	5.5	0.5	0.091
12	8.5	0.2	0.023
10.2	13.5	0.175	0.013

The value of m is plotted as a function of the voltage V in Figure 3.12 , and, as expected, the experimental results are well approximated as a parabola. This approximation is calculated using the least square method, obtaining:

$$m = \frac{1}{2742.6} \cdot V^2$$

¿From this equation we that, for any given value of the degree of mixing δ_m, the required length ℓ of the channel is given by the following expression,

$$\ell \simeq \frac{\delta_m}{V^2}$$

This dependence of the length of channel from the square of the voltage, together with the uninfluence of the polarity of the field applied, suggests that the instability process is driven by the energy of the field.

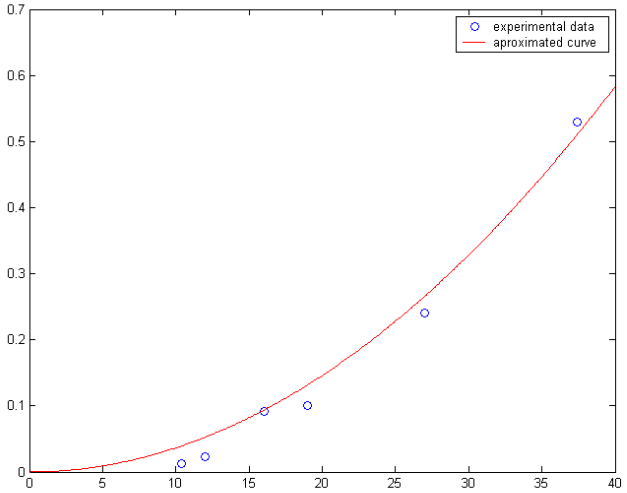

Figure 3.12: Plotting of the m value

Bibliography

[1] Ahmed Ould Moctar, Nadine Aubry and Jonh Batton *Electro hydrodinamic micro-fluidic mixer* , Lab on Chip, 2003, 3, pag 273-280.

Chapter 4

Pulse mixing through Electro Osmotic Flow

4.1 Introduction

The objective of this series of experiments is to show that mixing in microchannels can be strongly enhanced by using AC electro osmotic effects. This devices are proved to achieve high pressures into MEMS devices; moreover, using an alternated voltage, we obtain a pulsing effect in the liquid flow augmenting the mixing efficiency. Advantages in using this approach, compared to mechanical micropumps, are the lacking of moving devices and of any complex geometry design of the channel, resulting in lower costs. Two exemples of complex geometry are 3 dimensional twisted pipe (Figure 4.1)

and a staggered series of asymmetric herrigebone ribs along the floor of a 3 cm long channel (see [1] and [2]). In this experiments we used two physical phenomena, namely electro osmotic effects, for driving the flow, and pulse mixing, in order to augment mixing inside the micro device.

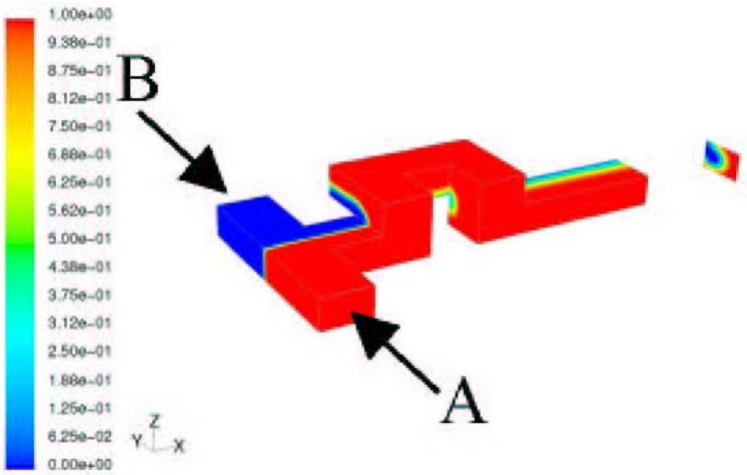

Figure 4.1: Mixing in a 3-D twisted pipe, from [2]

4.2 What EOF is

The Electro Osmotic Flow (hereby referred as EOF) is a technique to create pressure, and consequently a flow, within a channel; the basic idea is to apply an external electric field between the two ends of a channel, so that the ions within the fluid are subjected to a force, dragging the liquid and inducing a net flow. Naturally, in order to have a mean net velocity, either positive or negative ions must be prevalent. Now, a characteristics of some materials,

such as glass or plastic, is that, when they are in contact with a liquid, they gain a surface negative charge, especially if the liquid is an electrolyte. In fact,the channel walls act actually as a surface capacitor, with a constant charge and no net current moving from or toward the liquid. At the surface, an electric potential, called the 'Z-potential' is induced,

$$\zeta = \frac{\sigma_q}{\varepsilon_w \cdot \kappa}$$

where σ_q is the surface charge density at the channel wall, ε_w is the liquid permittivity, and $\kappa^{-1} = \lambda_D$ is the Debye length. This later is defined as the thickness of the electric double layer (EDL), or Debye layer [3], which is induced by the negatively charged walls, attracting positive ions. Basically, this 'ion cloud', of thickness λ_D, create a field that screens the field generated from the channel wall. Therefore, an EOF exists whenever an electric field is applied to the two ends of a channel with glass or plastic walls and containing an electrolytic fluid. In the past, this effect has not been studied extensively because, like any other surface effect, it is negligible in macroscopic channels. More recently, however, the study of EOF in capillary-size channels has become an important research topics, with the objective to enhance mixing and/or pumping in MEMS devices.

The EOF has a different velocity profile compared to laminar or turbulent fluxes, depending on the ratio between the channel half-width a and the

Debye length λ_D . In our case, assuming

$$a \gg \lambda_D,$$

the flow can be considered uniform, apart from a border region, with no-slip boundary conditions at the walls. In fact, since the fluid motion is due to the force exerted by the external field upon the free ions, with the field generated by the channel walls screened by the Debye layer, the ion concentration can be assumed constant.

4.2.1 The Equations of Motion

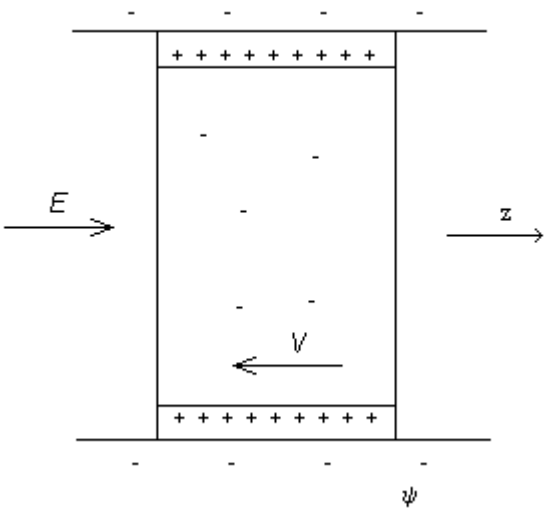

Figure 4.2: Scheme of the channel section

The electric osmotic flow is governed by the following equations:

$$V(y) = \frac{\Delta P/\ell}{2\eta}(a^2 - y^2) - \Omega \cdot E_z[1 - O(y)]$$

$$\Omega = \frac{\varepsilon_w \cdot \zeta}{\eta}$$

where V is the fluid velocity along the axial direction, y the distance from the center of the channel a is the half width of the channel and ℓ its length, ΔP is the pressure drop and η the fluid viscosity, E_z is the electric field. Here the first term represents the laminar flow term and the second is the electro osmotic flow term, with $O(y)$ representing a negligible term, that shapes the profile to 0 near the walls. This expression reduces to:

$$V = -\Omega E_z,$$

where we assume that both electrical field and ion concentration are homogeneous within the cross section. The minus sign is due to the fact that the flow has opposite direction with respect to the electric field, due to the negative charge of the free moving ions (Figure 4.2).

Since the flow is laminar, the pressure drop is proportional to the velocity and therefore the problem is linear. Consequently, if the $E(t)$ is a step signal of amplitude E, the velocity will be:

$$V(t) = -\Omega \cdot E \cdot (1 - e^{-\frac{t}{\tau}})$$

with τ depending on the mass of system and the fluid viscosity η. Since both Ω and τ are difficult to evaluate theoretically, we will try to determine them by measuring the transient response of the system.

Another way to study this phenomenon is by observing that the liquid has a volumetric density charge $\rho(y)$ which depends on the geometry of the channel (i.e. the ratio between the solid-liquid area surface and the liquid volume), and the concentration of free ions, the latter depending on the zeta potential at the interface due to de-protonation. Actually, we saw that the deionized water has already enough ions that this last parameter does not have any effect, so that $\rho(y)$ can by approximated as uniform, ignoring the borders.

At equilibrium, pressure loss and EOF pressure must have the same magnitude. Now, consider that the pressure drop in a channel of length ℓ is given by

$$\Delta P = -\frac{3\eta}{a^2} V\, \ell,$$

while the force applied by the electrical field E to a volume $2aW\ell$ of liquid is:

$$F = Q\, E = \rho A \ell E,$$

where W is the channel width and $A = 2aW$ the area of its cross section.

Therefore, since $\Delta P = F/A$, we conclude that

$$V = -\frac{a^2}{3\nu E}, \quad \Rightarrow \quad V \propto E.$$

4.3 What Pulse Mixing is

The problem of mixing in microdevices is not trivial, since at low Reynolds number (usually associated to microdevices) the flow is obviously laminar and the larger-scale methods of mixing do not work due to the pre-eminence of viscous damping. In general, microscale mixing between miscible fluids occur without the benefit of turbulence, by molecular diffusion alone. However, while diffusion of typical liquids (i.e. with diffusivities $D \simeq 10^{-5}\, cm^2/s$) could be fast enough for microdevices with smaller characteristic dimension ($10\mu m$ - $100\mu m$), in our case it is not appreciable, for diffusivity for most biological molecules is of $O(10^{-8}\, cm^2/s)$. In Figure 4.3 is shown what happens in microdevices when the only mixing is due to diffusion. In order to obtaining mixing, in the large problem class of low Reynolds number fluids, a common and already exploited solution is using chaotic advection ([5]). Chaotic advection consists of moving inert particles, which can only be dragged along with the fluid, in complex trajectories; this result in dispersing the particles, stretching, for example, a drop of dye into lines. In our device, Chaotic Advection is obtained by superimposing the main flow to a pulse

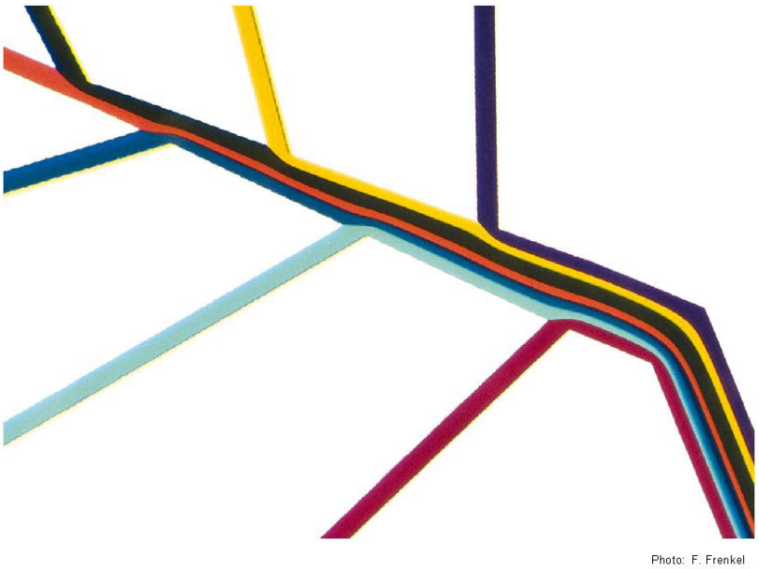

Figure 4.3: Laminar flow in micro channels (*George Whitesides Group,Harvard*)

flow inside the channel; however, without a main, net flow, the only result would be to displace the pure water-dyed water interface back and forth into the inlet channels without obtaining any mixing. This means that the particles are caught into a stagnating trajectory, where the particle position is a periodic function of time. When a a main, net flow is added, the particles are dragged toward the outlet, so that the stagnation is broken, the trajectory is no longer periodic and two adjacent points could move along diverging direction, causing the 'stretch' of our interface, and therefore, mixing.

4.4 Description of the Experimental Setup

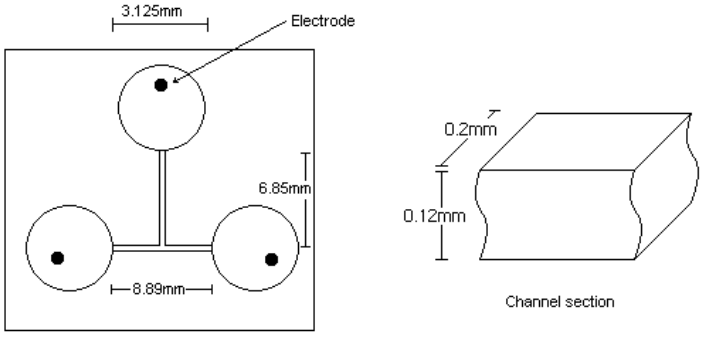

Figure 4.4: T-junction device drawing

The device is composed of a T-junction channel with 3 tanks at the end of each channel (Figures 4.4 and 4.5). A platinum electrode is placed in every tank, and a voltage is applied to each electrode.

4.5 Estimation of other forces acting in the device

4.5.1 Pressure due to gravity

First, let us evaluate the influence of gravity, considering that the two inlet tanks (of length $\ell_i = 4.45\,mm$) are both $1mm$ higher than the outlet tank (of length $\ell_o = 6.85\,mm$) and that the inlet velocity is half the outlet velocity.

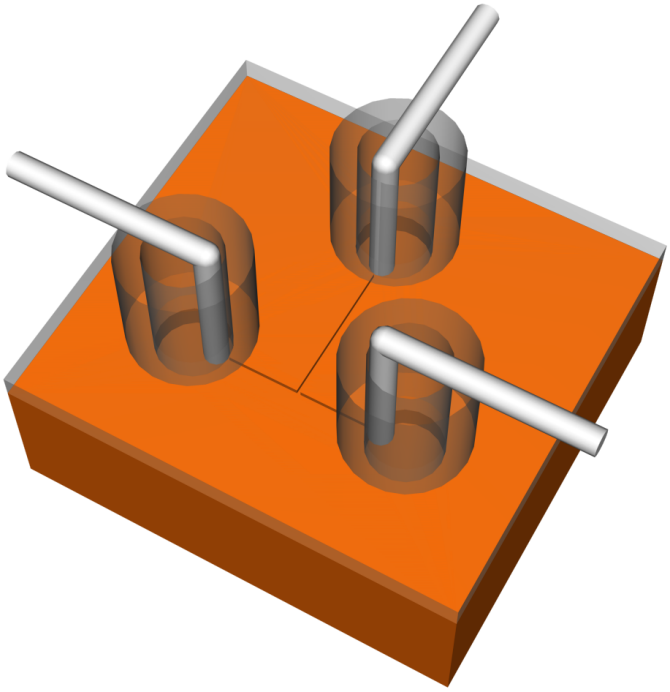

Figure 4.5: 3D T-junction device drawing

As we saw in the previous paragraph, the pressure drop for each segment is

$$\Delta P_{loss}(V, \ell) = -3\frac{\eta V}{a^2}\ell.$$

Finally, imposing that the pressure drop equals the static pressure head:

$$P_{Head} = \rho g \Delta h,$$

ignoring the pressure loss due to the T-junction, we obtain:

$$V \simeq 300a^2 \sim 10^{-6}\, m/s,$$

where we have assumed that $a = 0.1$. Therefore, we see that, since

the experimental velocity, as shown in the following chapters, are 2 orders of magnitude higher, we can safely assume that gravity does not have any effect on the flow.

4.5.2 Surface tension

When one or both the tanks run out of water, we will have air-water interfaces, and consequently we will have to consider surface tension effects inside the channel. This induce a drag force, which is given by the Young-Laplace expression,

$$P_{s,channel} = F_s/A = -\sigma/a.$$

Since the surface tension σ for air-water interfaces is $0.072N/m$, we obtain $P_{s,channel} \simeq 10^3$, which is therefore stronger than other effects. Consequently, as the transient flow field that arises when filling the device is very difficult to predict, we will assume that all the tanks contain at least some liquid and therefore air-water interfaces are not present.

4.5.3 Current loss

The liquid that we have used consists of deionized water (not pure, otherwise EOF would not work), therefore the resistance is high and can be assumed that the movement due to liquid transported charges do not affect the flow.

4.6 Device Modeling

In this small device, even not counting the disturbing forces that are listed above, it is difficult to take into consideration every aspect of the phenomenon, writing an accurate analytical model. In fact, many parameters are unknown: the channel roughness, the exact electrical field at every channel point (because the electrodes are not fixed), the current that flows into the channel, however small, etc.

4.6.1 Pressure due to gravity

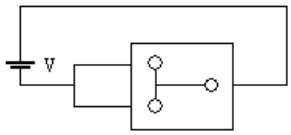

Figure 4.6: Schematic for velocity measurements

In order to obtain at least an experimental correlation, the fluid velocity has been measured as a function of the electric voltage, both at steady state and with step response. To do that, the two inlet electrodes were charged negatively, while the outlet electrode was charged positively (Figure 4.6). In the tables below, the resulting measurements are shown.

Transient Velocity after a $91.5\,V$ voltage was applied for 5 second.

t (s)	6.53	7.6	8.5	10.4	11.4	13.5	21.6	24	31.3	39.4
v(mm/s)	0.135	0.135	0.15	0.18	0.187	0.3	0.39	0.45	0.51	0.6

Steady flow Velocity (in mm/s)

Voltage	Min V	Max V
127	0.8	1
91.5	0.6	0.7
54	0.4	0.5
37	0.31	0.35

In Figure 4.7 the Transient velocity data were plotted and confronted with two exponential curves, both with $\tau = 15$s, and amplitudes 0.6 and 0.7 mm/s, in Figure 4.8, and with the origin of the $x-$axis placed at 5 second (i.e. when voltage is applied), in Figure 4.8.

Our experimental results are fitted reasonably well through the following correlations, valid at steady state and transient conditions, respectively,

$$V_z = -\Omega\, E,$$

and

$$V_z(t) = -\Omega\, E\left(1 - e^{-\frac{t}{\tau}}\right),$$

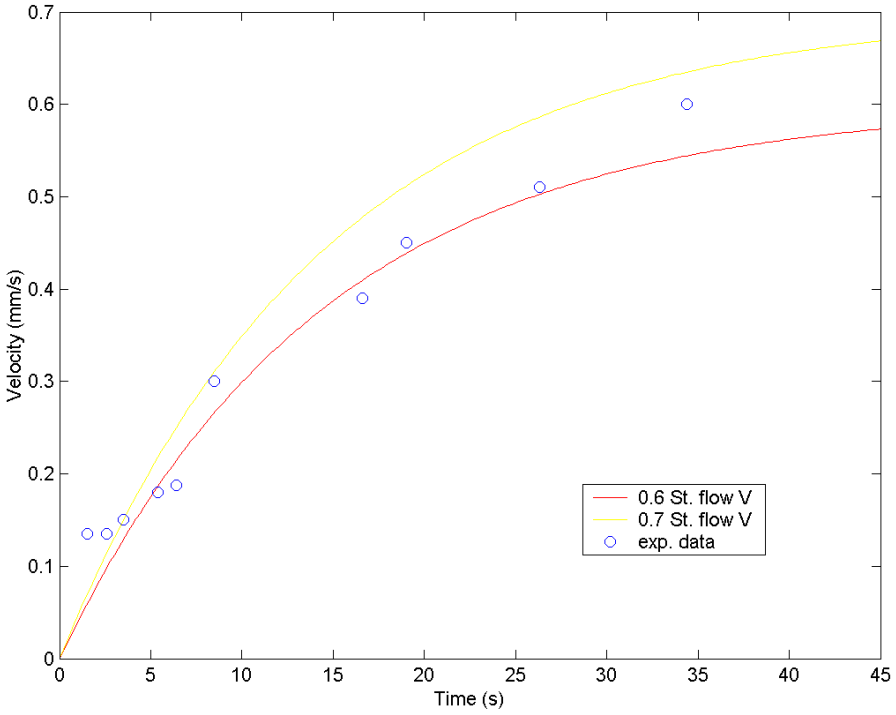

Figure 4.7: Plotting of the transient velocity for V=91.5 volts

where Ω is a dimensional constant,

$$\Omega \simeq 7.5\,10^{-6}\frac{m}{s^2\,V},$$

while, as we have already mentioned,

$$\tau \simeq 15\,s$$

It should be stressed that the numerical values of the two parameters Ω and τ given above are significant only for this very device. In the following, we will use these findings to understand which frequency and voltage amplitude

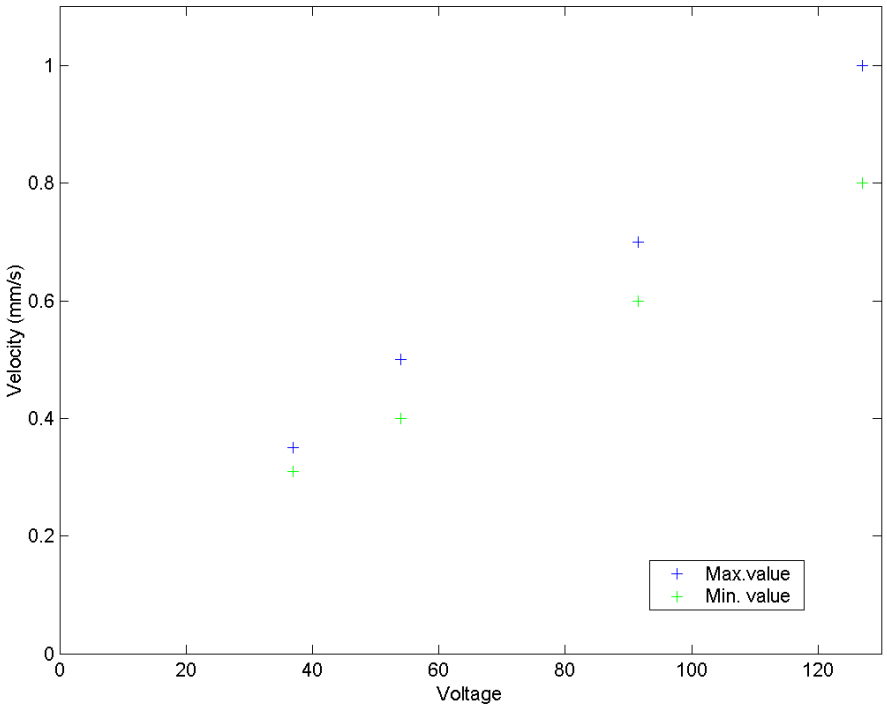

Figure 4.8: Plotting of Steady flow velocity versus Voltage

should be the chosen to enhance the mixing process.

4.7 Device Setup

Our goal is to demonstrate the efficiency of pulse mixing through EOF, so the first step is to create a flow that can be switched between a steady flow and a pulse flow.

In order to achieve this, the device is linked to the power supplies as shown in Figure 4.9. The DPDT relay, commanded by a square wave generator and

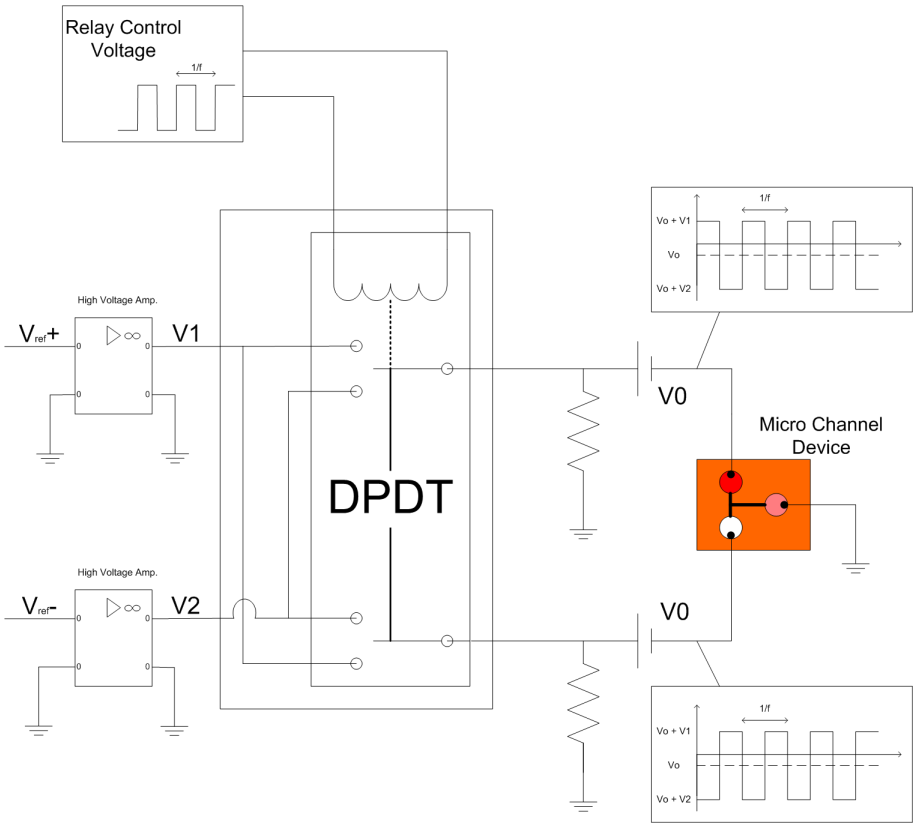

Figure 4.9: Device and power supply Schematic

with the pin connected as shown, permits to alternate input and output. First of all, we can safely assume that the current is almost zero, since the resistance measured between the two inlet electrodes is $15M\Omega$, while that between one inlet electrode and the outlet is about $21M\Omega$. Then, when both the amplifiers are off (High impedance, the system is powered from the two packs of batteries, with the "plus" grounded and the "minus" linked to the electrodes. Instead, when the amplifiers are both switched on, the effect of the resistance becomes negligible, as the generators have enough power

to supply both the system and the two resistances, and the batteries (V_0) can be considered in series with the amplifiers. Actually, since during the experiment the voltage $V1 = -V2$, the voltage of the electrodes when the generators are on is represented in Figure 4.10. If the generators are off, instead, the voltage is equal to Vo for both electrodes.

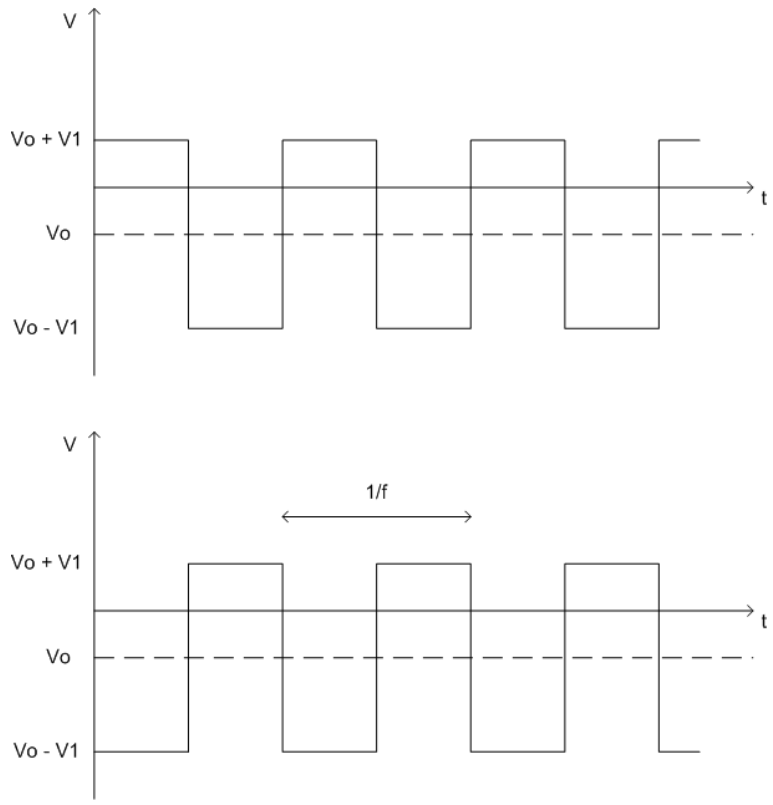

Figure 4.10: Voltage at the electrodes

4.8 Model deviance from real device

From a comparison between some experimental observations and a MatLab simulation emerged that, when the channel electrodes are powered with the AC signal, the experimentally measured velocity results larger than predicted. This error is due to two facts: the electric field is not constant, and the pressure loss is less in the channel that links the two inlet than in the whole channel. The main problem is that, while the electric field E and the fluid velocity V are linked by a linear relation, by changing the pressure loss due to the channel geometry and the velocity changes the characteristic time and the steady flow velocity value. The relations between electric field, pressure drop and velocity are:

$$\beta \dot{V} + \alpha \nabla P \ell V = 0$$

$$\gamma E + \alpha \nabla P \ell V \, (t \to \infty) = 0$$

Where ∇P is the pressure drop per unit length, while α, β and γ are dimensional constants.

Variations on the channel geometry (from the whole channel to the channel included between the two inlets) makes ℓ and E not constant.
Finally, from the two equations we obtain:

$$\tau \propto \ell$$

$$V_z(t \to \infty) \propto \frac{E_z}{\ell}$$

Although a comparison between ℓ of the entire device and that of the channel between the two inlets can be worked out, we do not know how any change in ℓ will influence the voltage. In fact, till now, E has been considered more like an input signal than a real field. In fact, understanding how much the electric field can increase with constant input voltage implies the knowledge of the field in every point.

The most straightforward way is consider the two configuration as straight channels with a variable field. remembering that we are working with an incompressible fluid, so the velocity must be constant,as wrote before, the velocity, in a section with a constant field and in steady flow condition, is proportional to the field, and proportional to the inverse of the pressure loss, that linear related with the channel length. The electric field can be considered constant into a section of the channel, and depends only from the $1/r^2$ variable, and we can reduce the channel to a 1 dimensional model, assuming the surface area as a multiplicative constant, too. It's reasonable to assume that the velocity in a entire channel is proportional to

$$Vel \propto (\int_0^\ell \frac{1}{r^2} dr)/\ell$$

Since our goal is to compute a ratio between two homogeneous values, all the constants that appear in the equations of the electric field can be omitted. The schematics are shown in Figure 4.11. The first one has been already used for calculate the main velocity; the latter is involved in the mixing process. The E field in the channel between in the two inlet is represented

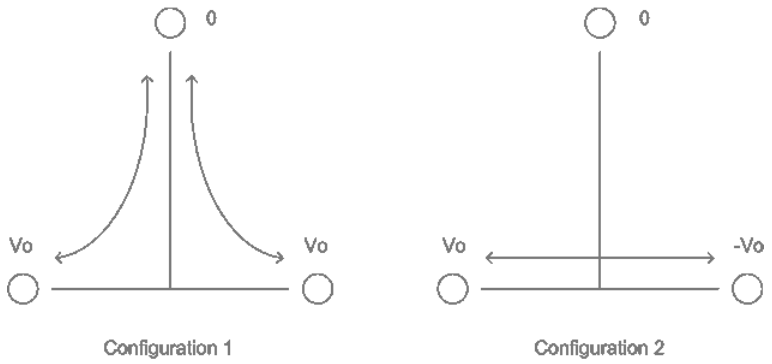

Figure 4.11: Schematic of the two configuration considered

qualitatively in Figure 4.13; In the first configuration the integral of the field is:

$$E1 = \int_{1.55}^{8.89} (\frac{1}{r^2} - \frac{1}{(3 + 8.89 - r)^2}) \cdot dr \simeq 1.1.$$

Instead, for the second configuration:

$$E2 = \int_{1.55}^{8.89} (\frac{1}{r^2} + \frac{1}{(3 + 8.89 - r)^2}) \cdot dr \simeq 1.18$$

While in this second configuration the electric field into the outlet channel is perpendicular to the channel, so that it can be considered equal to zero, in the first case the field is parallel to the outlet channel, although weak. the

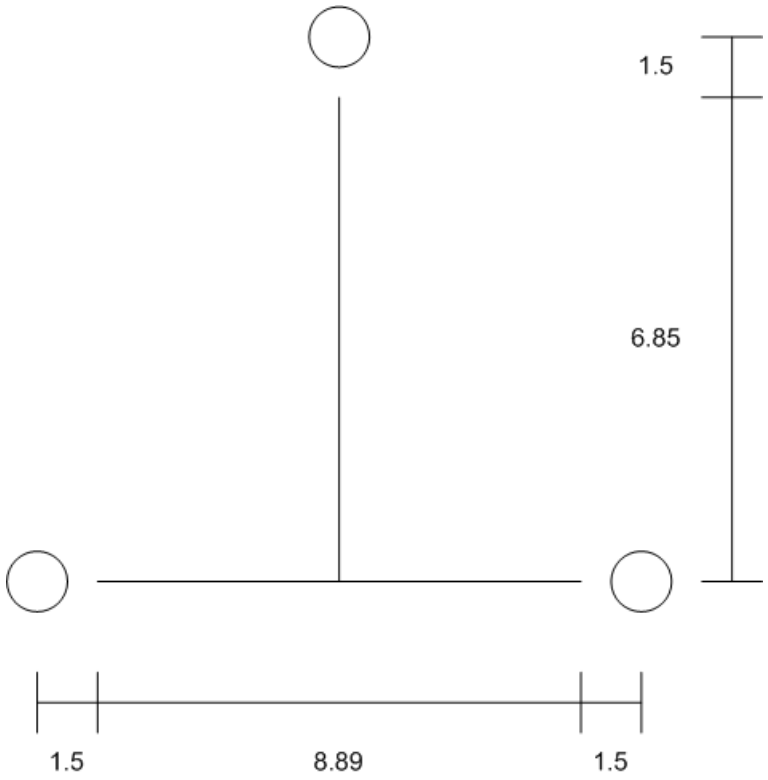

Figure 4.12: Drawing of the model used in computing the field (length in mm)

integral along the channel divided by the length of the channel is two orders of magnitude less than this same ratio evaluated at the inlet channels. The two integrals have to be divided by the length of the channel interested; in the first case the whole device, in the second the channel between the two inlet:

$$\ell 1 = 8.89mm + 6.85mm = 15.74mm$$

$$\ell 2 = 8.89mm$$

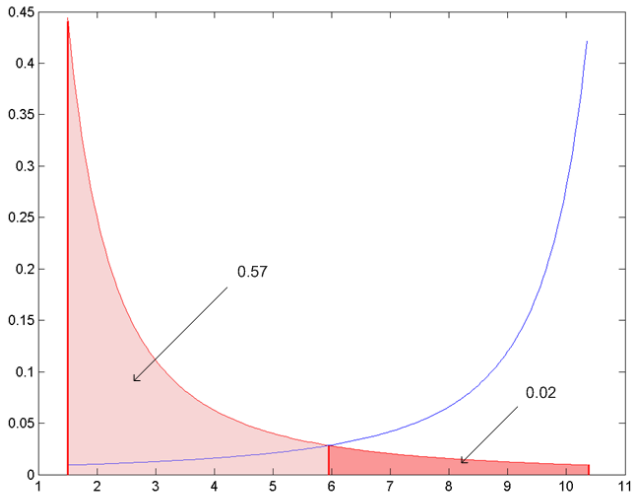

Figure 4.13: qualitative representation of E field between the two inlet

$$\tau 2 = \tau 1 \cdot \frac{l1}{l2} \simeq 8.5 sec$$

$$Vel2 = Vel1 \cdot \frac{l1}{E2} \cdot \frac{l2}{E1} \simeq Vel1 \cdot 1.9$$

Where $Vel1$ is the velocity calculated for main flow, $Vel2$ the velocity that should be obtained using the voltages as shown in Figure 4.11, Configuration 2.

After running a velocity measurement with voltages applied as in Configuration 2 (see Figure 4.11), the results confirm what was mentioned above: applying a voltage $\Delta V = 127\, Volts$, a velocity of $0.75\, mm/s$ (while we should expect a velocity between 0.8 and $1 mm/s$) and a relaxation time of about 13 seconds, (that is near half the time necessary for the other configuration). The imprecisions between the experimental and calculated data can

be attributed to some assumptions: In fact the electrodes are not fixed, so the electric field may vary from experiment to experiment; in addition, in configuration 2, we are assuming no movements into the outlet channel.

4.9 First approach of experimental mixing

During this experiment the two sets of batteries used for generate the steady flow supplies 58 volts on average[1]. In the experiments we have used a Rhodamine florescent dye to visualize the mixing dynamics: while one of the inlet tanks was filled with water, the other one was filled with a solution of dyed water, with a concentration of 1%. Lower concentrations proved to generate too dark images, while with this concentration it is fairly easy to distinguish the two different colors, but is difficult to catch the mixing, in the sense that hardly appear a zone with a color between red and black; in fact, the florescence dye tend to saturate the camera colors, causing a loss in information. Standard dyes has been tried as well, but the velocity of defusing is too high, the dye spread into all the tanks and the the mixing is not clearly monitored. Pulse mixing is shown in Figures 4.14, 4.15, and 4.16

[1]Since the the wave generator that drives the relay works even when the two amplifications are off (so the batteries switch between the two electrodes), a difference of some volts in the voltage supplied is not visible

for a $0.75Hz$ frequency and in Figures 4.17 and 4.18 with a $1.5Hz$ frequency.

4.10 Experimental and expected results

The experimental results do not agree with our predictions. In fact, trying to superimpose the steady flow velocity with the velocity caused by the pump mixing is clearly wrong, since the acceleration time (i.e. half of $1/f$,where f is the square wave frequency) is too short to reach steady state. So, while the velocity measurements between the two inlets agree with the expected values, the dynamics of the mixing cannot be determined so easily, so that we can conclude that a more detailed dynamical model should be determined. In the next chapter, we will briefly discuss some numerical simulation results, where we have tried to characterize the mixing process, albeit only qualitatively, given the impossibility to obtain data from images.

4.11 Theory of mixing and numerical simulation

In this section we will resume some of the information already published in [6], describing the fundamental parameters that influence the mixing process.

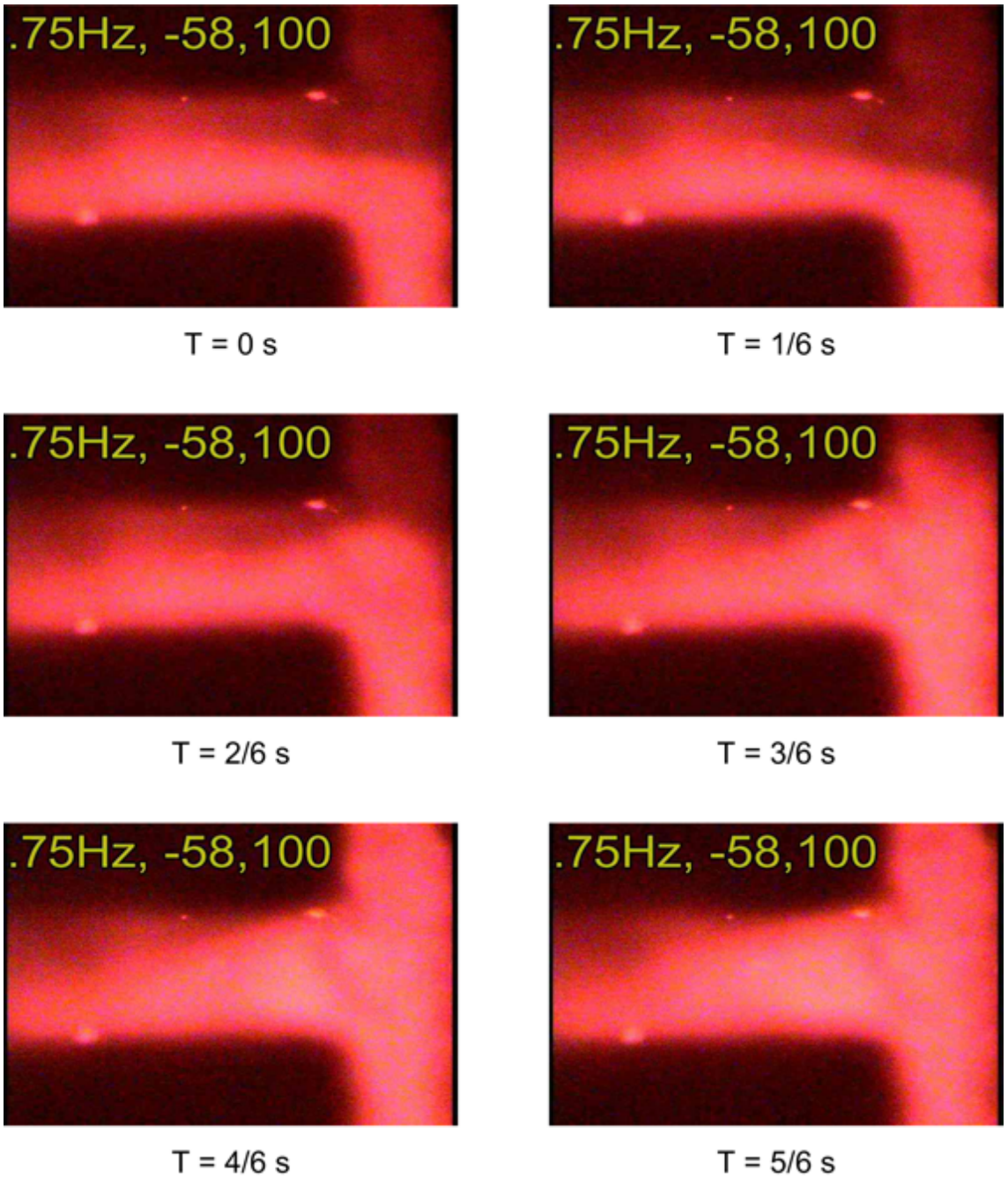

Figure 4.14: Pictures of mixing $(0.75Hz, 58 \pm 100V)$

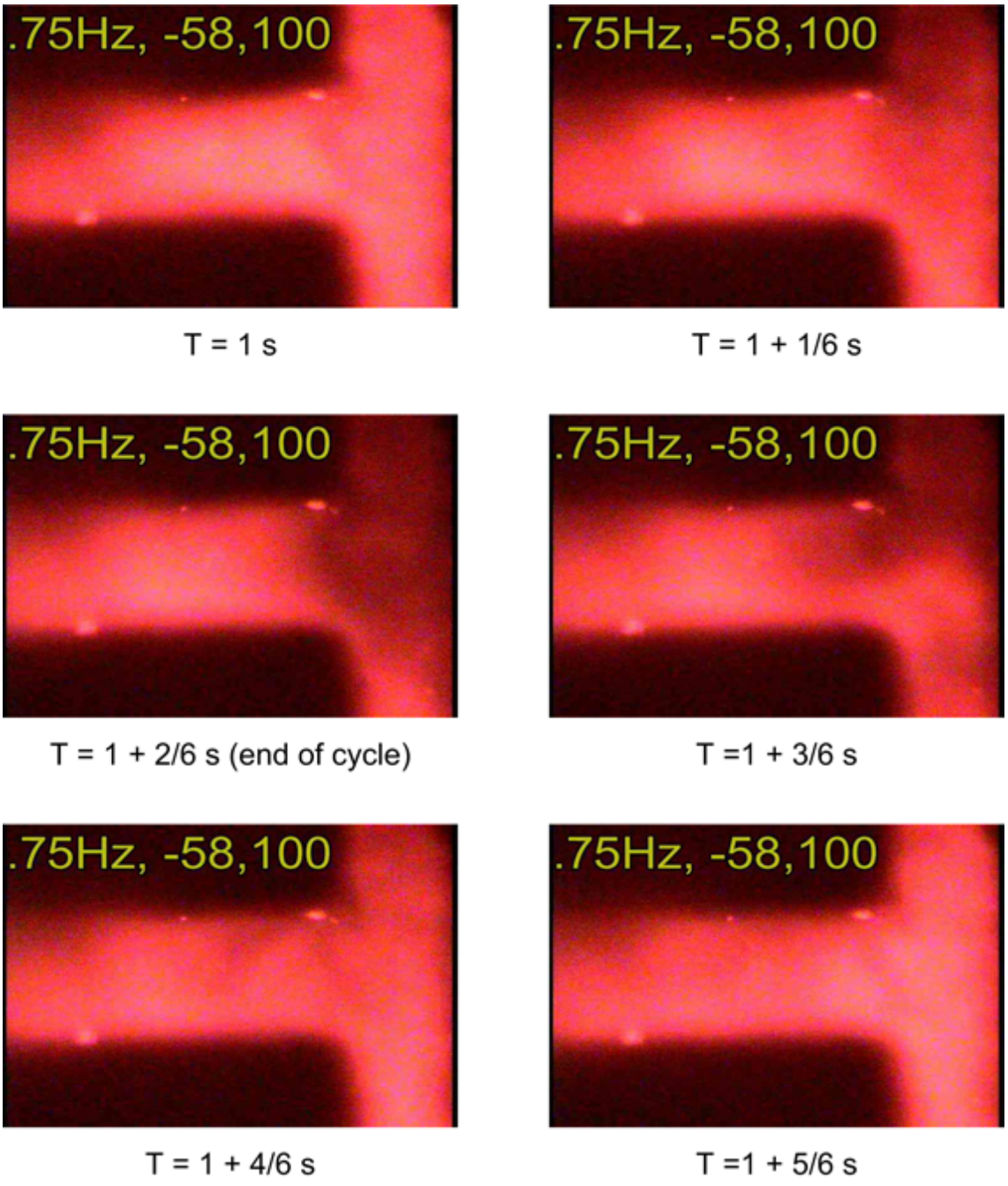

Figure 4.15: Pictures of mixing $(0.75Hz, 58 \pm 100V)$

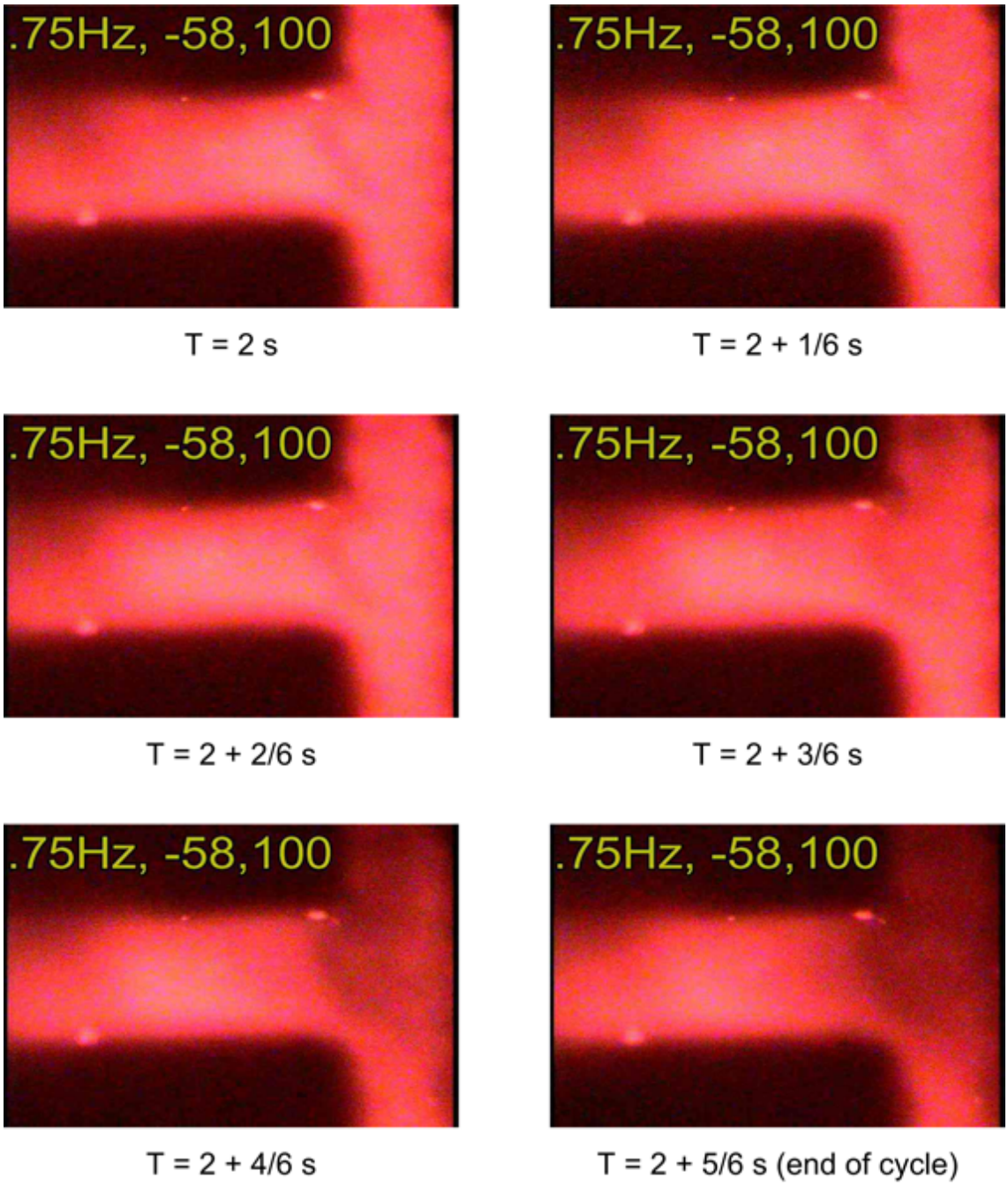

Figure 4.16: Pictures of mixing $(0.75Hz, 58 \pm 100V)$

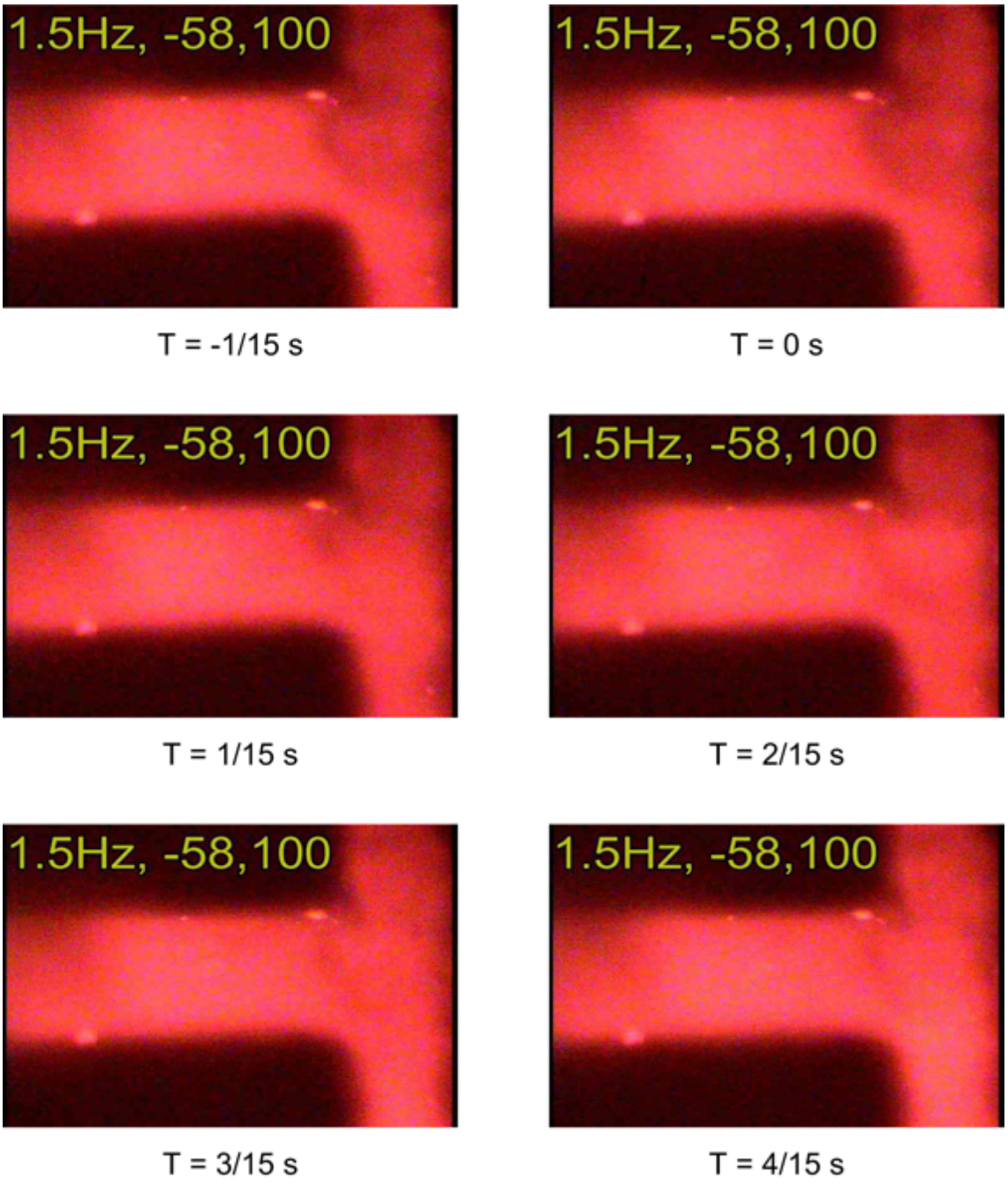

Figure 4.17: Pictures of mixing $(1.5Hz, 58 \pm 100V)$

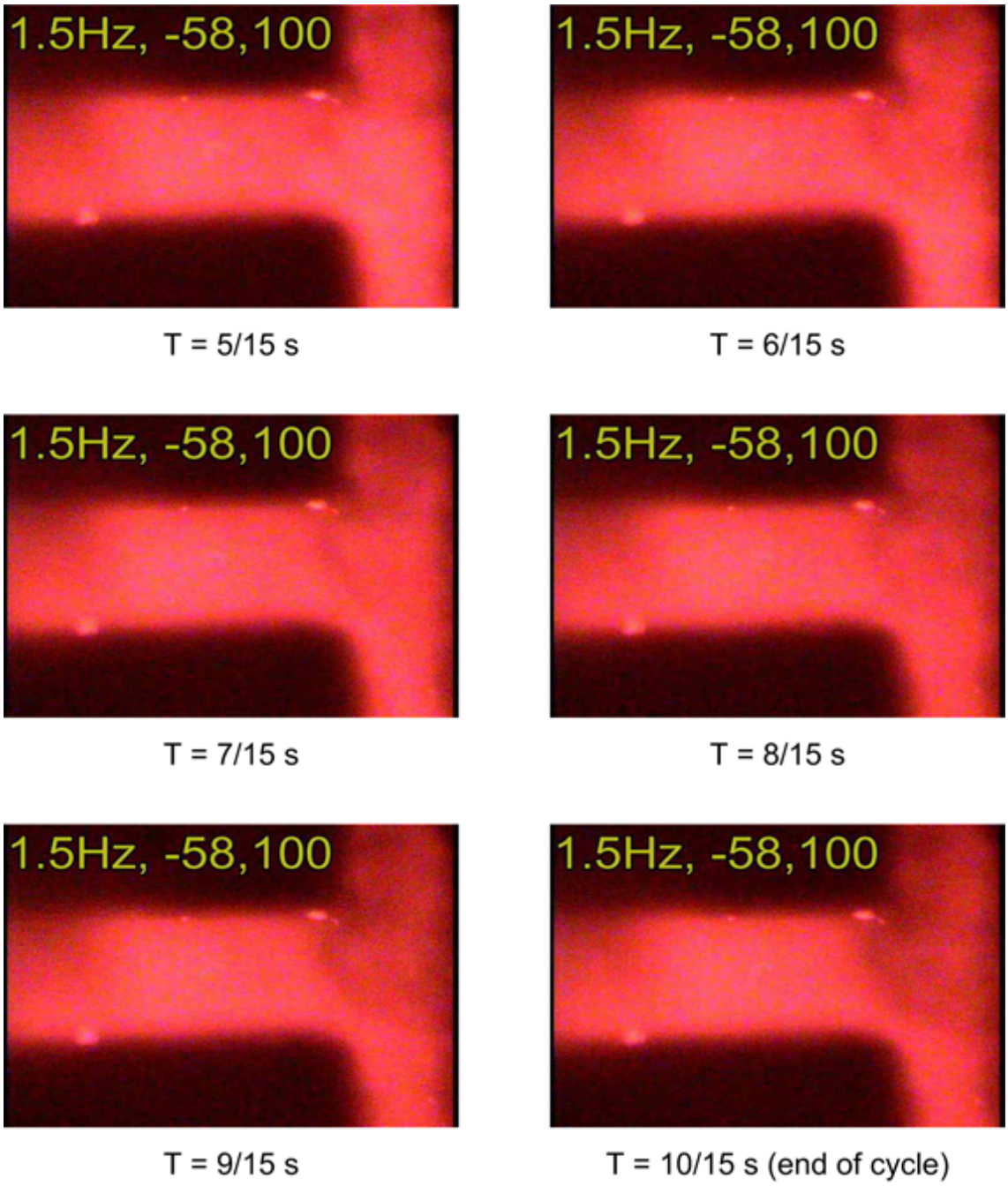

Figure 4.18: Pictures of mixing $(1.5Hz, 58 \pm 100V)$

This article present a study on pulse mixing properties on a T-channel, where the flow is controlled by external forces. One of these parameters is of course the Reynolds number,

$$Re = \frac{V\,L}{\nu} = 32 \times 10^{-3},$$

where $V = 2mm/s$, L is the hydraulic diameter,

$$L = \frac{4 \times Area}{(Wetted\,Perimeter)} = 16.2\,\mu m$$

and $\nu 10^{-2} cm^2/s$ is the water kinematic viscosity at room temperature and atmospheric pressure.

In this study it was found that in the case of pulse mixing the Reynolds number is not monotonically related to mixing.

Intermittent phenomena are often described through the Strouhal number, which is defined as the ratio between a characteristic time of the flow and the pulse flow period:

$$St = \frac{L/V}{1/f}$$

Since in the Strouhal number the volume of the displaced fluid does not play any role, we define another adimensional term, the Stokes number, which characterizes the ratio between the fluid velocity and the displaced fluid volume. More exactly, the Stokes number is the ratio between the characteristic time that is necessary to establish a fully developed velocity field, i.e. (L^2/ν)

and the pulsing time period,

$$Sto = \frac{L^2/\nu}{1/f} = St \cdot Re$$

From here we see that the Stokes number is not independent, but it is the product between the Reynolds number and the Strouhal number. A value of $Sto < 1$ means that the pulse is fully developed, while the maximum transport of liquid occurs for $1 < Sto < 5$.

The cited article also investigated whether the applied waveforms influence the mixing index; some tests have been run, holding velocities and frequency constant, resulting in no significant variations. Instead, a parameter that greatly influences the degree of mixing is the phase difference $\Delta\varphi$ between the pulses at the two inlets; till now only a π phase difference has been investigated, but we saw that when $\Delta\varphi = \pi/2$ mixing was greatly enhanced.

The latter fact brought us to change the driving voltage to a two sinusoidal waves shifted one from the other. The experiment results will be presented in the next chapter, but now we discuss the data obtained from computer simulations[2]. Computer simulations were conducted for a 3 dimensional T-channel, imposing the velocity of the fluid at both inlets (i.e. an impose boundary condition that varies with time, as a square wave or a sinusoidal

[2]Numerical simulations were executed by Dr. Ian Glasgow and Lee Carlson, and the data obtained were elaborated by Dr. Ian Glasgow and Dr. Nadine Aubry, at the New Jersey Institute of technology

wave) and, in order to simulate the peculiar profile of electro osmotic flow, the no-slip boundary condition were not applied to the channel wall, so as to obtain the flat flow profile that is observed experimentally (in fact, as shown in Section 2, the flow profile is almost uniform, with the exception of the very narrow Debye layer by the wall). The mixing index δ_m is the same defined earlier, hereby modified to fit the data obtained from computer simulation:

$$\delta_m(t) = 1 - \frac{I(t)}{I_{unmixed}},$$

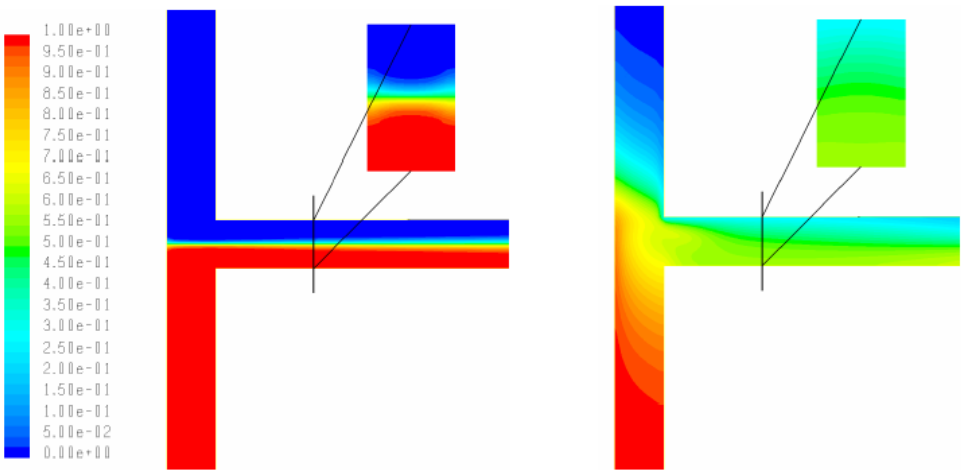

Figure 4.19: Example of simulation result, on the left no pulsing superimposed, on the right π phase delay sine wave superimposed

An example of simulation is reported in Figure 4.19.

The test was carried over by imposing the frequency ($f = 8Hz$), the mean flow velocity ($0.8mm/s$), and the peak velocity ($4mm/s$) at both inlets, using

for both tests square waves, and setting $\Delta\varphi = \pi$ and $\Delta\varphi = \pi/2$. After a while (about $3s$ for this choice of main flow velocity, and measuring the degree of mixing $5mm$ downstream) the mixing indexes reach the following constant values:

- For $\Delta\varphi = \pi$ the mixing index is 0.8

- For $\Delta\varphi = \pi/2$ the mixing index is 0.59

4.12 Experimental setup and result for $\pi/2$ lagged sine wave

After reviewing the results of the numerical simulations, we tried to reproduce them experimentally. After some attempts, we found that the best setup consisted in applying $[100 + 275\, sin\,(2\pi ft)]\, V$ and $[100 + 275\, cos\,(2\pi ft)]\, V$ voltages at the inlets, with $f = 8Hz$. Since the DPDT relay is no longer used, we can use larger voltages, and so higher frequencies are needed: referring to the parameters defined above, that means that both the Strouhal and the Stokes numbers are larger. Since we are not able to draw quantitative results, we did not worry about carrying on a parametric study, and instead of trying to choose a case that can be compared with the square wave experiment, we choose to display the best results that we found. Figure 4.20 reports some

results from this last experiment.

4.13 Conclusion

Pulsing demonstrated to be a good way to generate mixing, while Electro Osmotic Flow bring the advantages to eliminated moving parts, and cut off of the liquid volume needed to most pumping device to create a pressure. Experimental qualitative observation and computer simulation confirm that, the larger the number of pulse experience a particular plug of fluid, the greater the mixing. A plug can experience more pulsing changing frequency or the impulse driving voltage. We experienced a range of voltage high up to 300 volts, without creating any undesired effect in the liquid channel, as formation of bubbles. We found also that, since the energy absorbed by the the system is small, the whole process can be powered by batteries. While the modeling of a straight EOF pump it's easy and well documented, finding a suitable model to describe the flows into the T-device proved too difficult, and even computer simulation have to consider an imposed velocity as input instead the actual field, an hypothesis that, even if close to reality, cannot be at the moment checked. We also confirmed the relation between the delay of the 2 inlet signals and the mixing, even if the just the computer simulation can be accounted for that, since the difficulties with the florescence

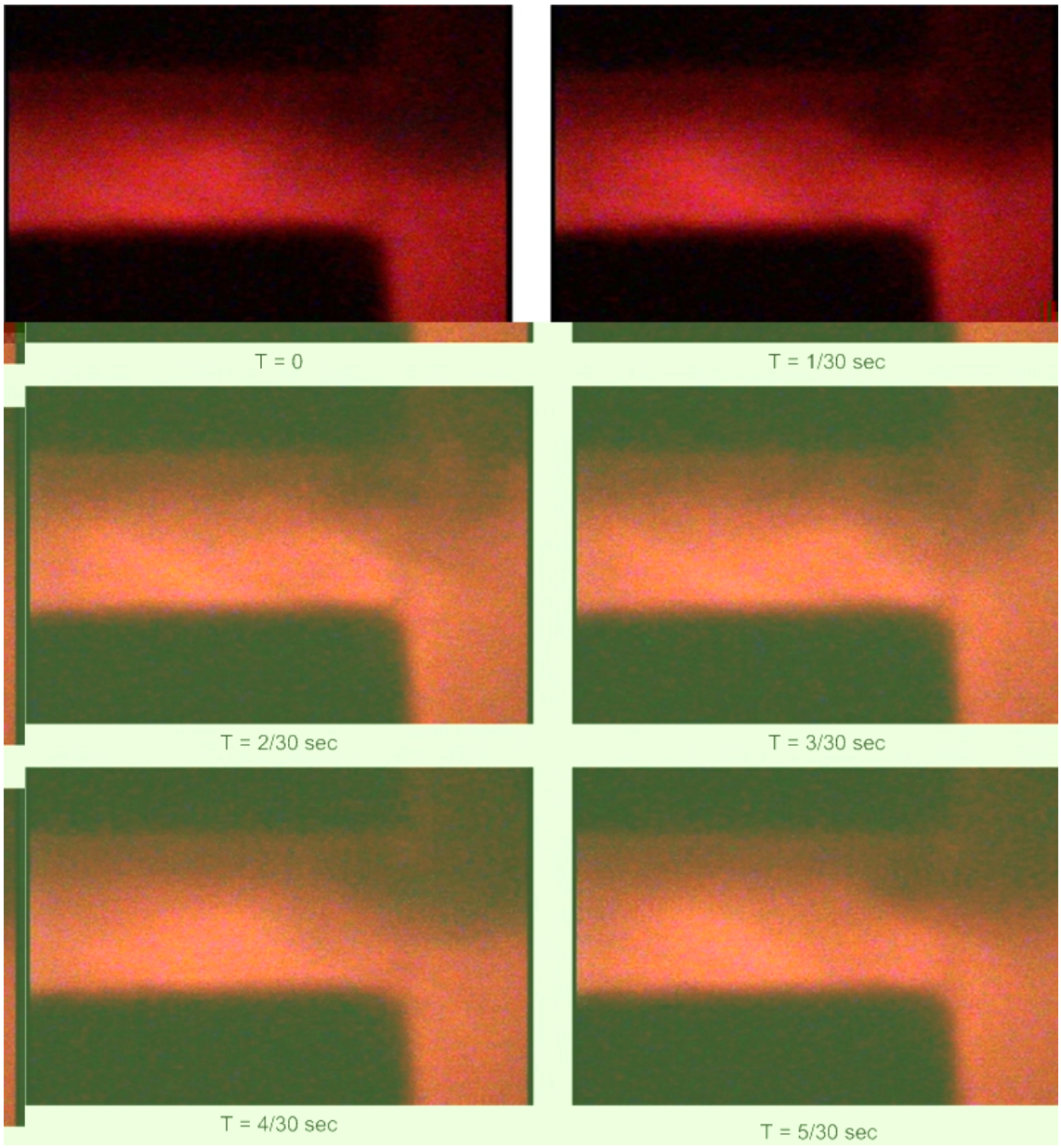

Figure 4.20: Pictures of mixing with a 90^o phase delay($100V + 275V \cdot sin(2\pi ft)$ and $100V + 275V \cdot cos(2\pi ft)$)

dye doesn't give as the opportunity for a parametric study.

Future development of this technology are in optimizing the flow velocity: Using a packed particles into the channel in order to augmenting the channel wall surface, thus augmenting the free ion concentration, and the velocity of the fluid, for the same voltage. An other method to operate on the concentration of free ion is to make part of channel into a symmetrical electric field; actually the walls already acts a capacitor, putting a real capacitor will give as the opportunity to control the ion concentration, that, in the limit of weak Z-potential is a linear phenomena (i.e. the relation between the ion concentration and the voltage applied is linear). At last, optimizing the shape of the electrodes that make the water flow, in order to not allow the field be dispersed outside the channel, and isolating the electrodes, cutting down any joule effects (and saving power) obtaining higher velocities with lower voltage, without the occurring of undesirable effects (like formation of gas bubbles).

Bibliography

[1] Liu, R. H., Stremler, M. A., Sharp, K. V., Olsen, M. G., santiago, J. G., Adrian, R. J., Aref, H. Beebe D. J., *Passive Mixing in a three dimentional Serpentine Microchannel*, Journal of Microelectromechanical System, 2000, 9, 190-197

[2] Stroock, A.D., Dertinger, S.K.W., Ajdari, A., Mezic,I., stone, H. A., whiteside, G. M., *Chaotic mixer for microchannel*, Science, 2002, 295, 647-651

[3] R.J. Hunter *Zeta Potential in colloid science, Principles and Application* , Accademic Press, New York, 1981.

[4] C.L. Rice, r. Whitehead, *Elettrokinetic flow in a narrow cylindrical capillary*, J. Phys. Chem. 69 (1965) 4017.

[5] Julyan H. E. Cartwright, Mario Feingold3, Oreste Piro *An Introduction to Chaotic Advection*, Mixing: Chaos and Turbulence, Eds. H. Chate, E.

Villermaux, J. M. Chomez, Kluwer, pp. 307342, 1999

[6] Ian Glasgow, Sam Lieber, and Nadine Aubry, *Enhancement of Microfluidic Mixing Using Time Pulsing*, Lab on a Chip, May 2003 issue

[7] T.M. Squires e M.Z. Bazant *Induced-charge electro-osmosis* Jornal of Fluid Mechanics (vol. 509, June 2004) pp. 217-252

Chapter 5

Acknowledgments

I want to thank Pr. Nadine Aubry, Mr. John Batton, and George Barnes for they availability and precious guide through this 6 month period at NJIT, Newark, NJ, and i owe thanks to Max Roman and Amit Banerjee (Bengali) for helping me in more practical matters. i also have to thank Ian Glasgow for letting me collaborate with him, and his helpful talks about Electro Osmotic Flow.